Ion Dynamics in a Linear High Field RFQ Trap

by
Omar Gianfrancesco

Department of Physics,
McGill University
Montreal, Canada

December, 2005

A thesis submitted to
McGill University in partial fulfillment
of the requirements for the degree of
Doctor of Philosophy

Library and
Archives Canada

Published Heritage
Branch

395 Wellington Street
Ottawa ON K1A 0N4
Canada

Bibliothèque et
Archives Canada

Direction du
Patrimoine de l'édition

395, rue Wellington
Ottawa ON K1A 0N4
Canada

Your file Votre référence
ISBN: 978-0-494-25155-3
Our file Notre référence
ISBN: 978-0-494-25155-3

NOTICE:
The author has granted a non-exclusive license allowing Library and Archives Canada to reproduce, publish, archive, preserve, conserve, communicate to the public by telecommunication or on the Internet, loan, distribute and sell theses worldwide, for commercial or non-commercial purposes, in microform, paper, electronic and/or any other formats.

The author retains copyright ownership and moral rights in this thesis. Neither the thesis nor substantial extracts from it may be printed or otherwise reproduced without the author's permission.

AVIS:
L'auteur a accordé une licence non exclusive permettant à la Bibliothèque et Archives Canada de reproduire, publier, archiver, sauvegarder, conserver, transmettre au public par télécommunication ou par l'Internet, prêter, distribuer et vendre des thèses partout dans le monde, à des fins commerciales ou autres, sur support microforme, papier, électronique et/ou autres formats.

L'auteur conserve la propriété du droit d'auteur et des droits moraux qui protège cette thèse. Ni la thèse ni des extraits substantiels de celle-ci ne doivent être imprimés ou autrement reproduits sans son autorisation.

In compliance with the Canadian Privacy Act some supporting forms may have been removed from this thesis.

While these forms may be included in the document page count, their removal does not represent any loss of content from the thesis.

Conformément à la loi canadienne sur la protection de la vie privée, quelques formulaires secondaires ont été enlevés de cette thèse.

Bien que ces formulaires aient inclus dans la pagination, il n'y aura aucun contenu manquant.

Canada

Abstract

A new linear high electric field radiofrequency quadrupole (RFQ) ion trap, dubbed HVTrap, was developed and tested to study the phase space properties of confined particles and determine the suitability of such a device as an ion source/delivery system for high-resolution time-of-flight (TOF) mass spectrometry and to test the possibility of high field RFQ beam cooling in an ion guide.

A segmented quadrupole rod structure was built and shown to easily withstand over 4kV between adjacent electrodes placed 1mm apart in 1×10^{-4} Torr of helium buffer gas. An innovative resonating circuit design using hollow air-cored induction coils was used to simultaneously deliver the necessary RF and DC trapping potentials to the linear RFQ system as well as deliver the extraction voltages used to eject test ions (Cs^+, m/z = 133) produced by a surface ionization source. The resulting ion bunches were delivered to a TOF system for time profile analysis using a multichannel plate detector. Optimal trapping parameters were found to vary with applied RF potentials and extraction voltages. The presence of helium buffer gas at pressures of 10^{-4} Torr and long cooling times, in the range of 500ms, were found to improve the number of detected ions.

A thermodynamic model of the confined ions was used to simulate the extraction process and follow the phase space evolution of the ejected particles through the TOF region. Analysis of the experimental data showed that confined Cs^+ ions reached equilibrium temperatures as low as 0.45 eV after 500ms cooling periods in 1×10^{-4} Torr of helium buffer gas. These equilibrium temperatures were also found to be dependent on the number of detected ions and applied RF potentials. Harmonic frequencies in the resonant circuit are thought to play an important role in determining the thermal energies of the trapped ions.

This thesis has shown that high field RFQ confinement of ions in buffer gas is indeed feasible and that trapped particles can be manipulated using DC fields superimposed on the RF. In its present form, the HVTrap would be capable of mass resolutions of roughly 1000. Beam cooling using a high field RFQ would also be possible and could potentially accommodate beam currents of up to 100nA. If the ion temperature could be reduced to 0.05 eV, TOF mass resolutions of 30 000 would be possible.

Résumé

Un nouveau piège à ion linéaire "RFQ" à haute tension, communément appelé "HVTrap", a été développé et analysé de façon à étudier les propriétés "phase-space" des particules confinées. Tout ceci dans le but de déterminer les exigences nécessaires pour utiliser un tel piège en spectrométrie de masse à haute résolution ainsi que refroidir des faisceaux radioactifs intenses.

Une structure segmentée à tige quadrupolaire a été construite et démontré à supporter plus de 4kV entre électrodes adjacent placés à 1mm de distance dans un gaz d'hélium à 1×10^{-4} Torr. Une circuit résonant innovateur utilisant des rouleaux inductifs creux a été employé pour distribuer les potentiels RF et DC simultanément de même que les potentiels d'extraction pour expulser les ions test (Cs^+, m/z = 133) produits par une source d'ionisation superficielle. Les groupements d'ions extraient ont été envoyé à un détecteur "MCP" via un système "TOF". Les paramètres optimaux du piège variaient selon les potentiels RF appliqués et les voltages d'extraction. La présence d'hélium gazeux à des pressions de 10^{-4} et des longues périodes de refroidissement ont amélioré le nombre d'ions détectés.

Un model thermodynamique des ions confinés a été employé pour simuler le processus d'extraction et poursuivre l'évolution du "phase space" des particules expulsées à travers la région TOF. Les données expérimentales démontrent que les ions Cs^+ enfermés ont atteint une température minimum d'équilibre de 0.45 eV après des périodes de refroidissement de 500ms dans un gaz d'hélium de $1x10^{-4}$ Torr. De plus, ces températures d'équilibre étaient dépendent du nombre d'ions détectés ainsi que des potentiels RF appliqués. Les fréquences harmoniques du circuit résonnant sont considérées comme une source importante d'énergie thermale pour les ions piégés.

Cette thèse démontre que confiner des ions à l'aide de hautes tensions dans un système "RFQ" est bien possible et que les particules emprisonnées peuvent être manipulé en superposant des potentiels DC et RF. Sous sa forme présente, le HVTrap serait capable d'une résolution de masse d'environ 1000 et pourrait potentiellement accommoder des faisceaux ioniques de 100nA. Si la température des ions peut être réduite à 0.05eV, des résolutions de masse de 30 000 pourront être possible.

Acknowledgements

I would like to begin by expressing my deepest gratitude to Prof. Robert B. Moore, “Ye Olde Master”. His tutelage and guidance over the years have been indispensable to the success of this project as well as to my education. He has been the central force behind this project providing the original motivation for this thesis as well as many of the basic designs needed to build the various components used throughout this project. I would like to thank him for his help with the modifications made to the original trapping system, for his help in developing a working zeolite heater for the surface ionization source and for the use of his random phase space coordinates generator. I would also like to express my appreciation for his help in writing and editing this thesis in addition to providing the use of his notes on electromagnetic traps and ion guides. Moreover, I would like to thank him for helping me rediscover my love for physics and for taking me under his wing at a moment when I was unsure of where I was going. Prof. Moore has been more than my supervisor, he has been my mentor.

I would also like to thank the many people that have helped me during my stay at McGill University and that have taught me the innumerable details not shown in the classroom. In particular, I would like to thank Leo Nikkinen for sharing his vast knowledge of electronics with me and for helping me design, build and test many of the electronic components used throughout this work. I would also like to thank him for helping me get over my fear of electronic circuits and for showing me the importance of a good circuit diagram; Mr. Steve Kekani and Mr. Eddie Del Campo for their help and guidance in building some of the components used in this project and for teaching me the finer points of machine shop work; C.W. Van Fong for “showing me the ropes” as a summer student in Prof. Moore’s lab and for introducing me to SIMION 3D; Ali Alousi for introducing me to vacuum systems and a number of vacuum techniques; Mario Della Neve, for providing me with sound advice on everything from vacuum systems to career paths; Michel Beauchamp, for helping me find “misplaced” equipment in the department all these years; Mohammad Ghalambor-Dezfuli, for his guidance in the initial setup of this project; to Ricardo Lambo for developing the cesium zeolite used in our surface

ionization sources; to summer students Pierre-Andre Gagnon and Marc-Antoni Goulet who's help with the RFQ simulations were invaluable; and to my friends, their constant jokes and taunts over the years at my attempts to "split the atom" or "build a time machine" have kept my feet firmly on the ground.

I would also like to thank Louise Decelles, Diane Koziol, and Elizabeth Shearon for their help in dealing with the innumerable university and departmental procedures over the years. To Paula Domingues, for helping me adjust to life as a grad student and for always having a smile every time I went to bug her with questions. Specials thanks must also go out to Sonia Vieira, my very own personal life-saver. She not only helped me deal with the bureaucratic red tape I had to face every time I placed special equipment purchase orders but she also humored me every time I tried flirting with her.

Finally, I would like to thank my family. Their unwavering support and encouragement throughout the years has allowed me to pursue numerous opportunities and confront many challenges that would have seemed too terrifying for me to take on alone. Thank you.

Table of Contents

List of Figures

List of Tables

Chapter 1 Introduction

Stronger, and at the same time more sensitive, experimental apparatus for measurements has been the life-blood of science all throughout history. The development of high-precision optical interferometers, for example, enabled Michelson and Morley to try to measure the velocity of the Earth through the ether and determine the place of the Earth relative to the center of the Universe. The unexpected result that the velocity of light in a vacuum was independent of the velocity of the Earth, or indeed independent of anything, is the underpinning of the theories of relativity that form the modern mathematical model of the structure of the Universe.

One of the most important set of measurements for determining the dynamics of matter in the Universe is that of the masses of the atomic nuclei. This is because they reflect the energies involved in the processes by which the solar systems of the Universe have evolved into their present form. The history of ever increasing accuracy and sensitivity of these measurements, from a beginning of about a part in one thousand, to the present accuracies of up to one part in a billion, is the history of the development of the present understanding of the nuclear forces that are involved in these processes.

High-sensitivity high-accuracy mass measurements of atomic nuclei are very much an ongoing project. At facilities such as ISOLDE at CERN and TRIUMF in Vancouver, the techniques are now being extended to short-lived radionuclei that only occur naturally in the interior of exploding stars. Their short half-lives and very low production rates at even the most powerful facilities require the very highest in sensitivity of such measurements.

The central element in modern high-accuracy high-sensitivity mass measurement apparatus is the Penning trap [Bol96]. This device enables measurements of accuracies approaching 1 part in 10^{11} on single ions. To achieve this, however, the trap must have the ion to be measured delivered to it very precisely and with certainty that it is indeed the desired ion. This imposes severe requirements on the apparatus that must take the atomic nucleus out of the target in which it has been created by a bombarding beam, sort it from the myriad of other ions that are emitted from the target, cool it so that it can be delivered with precision, and then direct it so that it can be captured in the measuring Penning trap.

This preparation and delivery of a radionuclide to a Penning trap cannot be carried out in one simple system. A typical system for accomplishing these operations is shown in figure 1.1. This is the ISOLTRAP facility [Bol96] at CERN, a pioneering facility designed for very high accuracy mass measurements on the very rare highly unstable radionuclides that are delivered by the ISOLDE facility as 60 keV ions from a magnetic sector mass separator in bunches of as few as 1000 ions every few seconds.

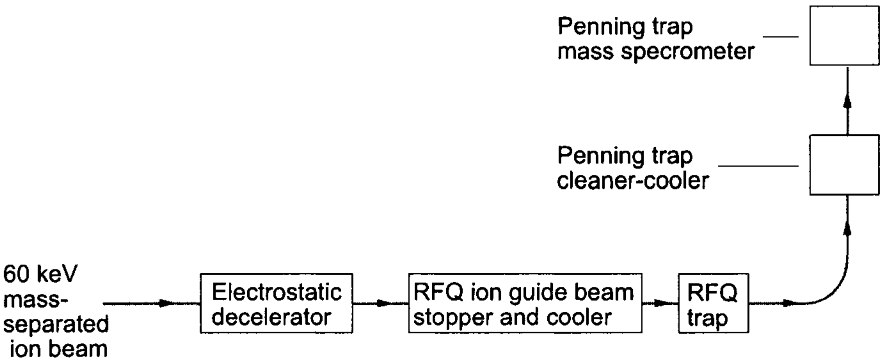

Figure 1.1 Schematic of the ISOLTRAP facility at ISOLDE at CERN.

Upon delivery to the ISOLTRAP facility these ions are electrostatically decelerated to about 50eV, whereupon they are captured in a radiofrequency quadrupole (RFQ) ion guide operating at sufficient background gas pressure to bring the ions to rest. The ions are then collected in an RFQ trap attached to the end of this system and delivered, on demand, as microsecond pulses to a subsequent electromagnetic trap for very high resolution filtering and cooling. This trap is a Penning trap, which achieves axial confinement by a static quadrupole electric field and radial confinement by a magnetic field. By using the cyclotron frequency of the ions, the filtering can reach mass resolutions ($m/\Delta m$) of up to several hundred thousand, allowing the removal of even isobars, such as O_2^+ from $^{32}Ar^+$. After purification and cooling the $^{32}Ar^+$ collection is then delivered to the actual mass measuring trap, which is an extremely high resolution Penning trap mass spectrometer. A recent result from this facility is the mass of ^{32}Ar, which is of great interest in both nuclear and astrophysics. The power of the techniques that are involved is shown by the accuracy of several parts per 100 million that was obtained from about 10,000 Ar^{32} ions that were delivered in the presence of about 10 million times as many ions of O_2^+.

The RFQ ion guide and trap are an essential component of this system. It is they that capture the ion beam for the first time, bringing it to rest so that it can be cooled in a buffer gas and then collect it for delivery as a bunch of ions, on demand, to the subsequent Penning cleaner-cooler trap. Without this pre-cooling and bunching the Penning cleaner-cooler would not work.

RFQ ion guides and traps are particularly suited for this application since they are capable of total confinement of ions that have a high dispersion of velocities, corresponding to kinetic energies of up to tens of electron volts, in an environment of light buffer gases such as helium that will quickly cool the ions to nearly the temperature of the gas. First conceptualized by Paul in 1953 [Pau53], RFQ ion confinement was initially used for the study of gaseous ions. It is now widely used in chemistry and physics, one of the most common uses being for the analysis of the residual gas molecules in a vacuum system, where the parameters of the confinement are adjusted so that ions formed from the molecules by electron impact will only be confined, and therefore detected, if they have a specific mass. (The device is commonly referred to as a "residual gas analyzer".) The versatility of the RFQ ion confinement technique is shown by another common use in mass spectrometry in biomolecular research; the triple sequential mass spectrometer shown schematically in figure 1.2.

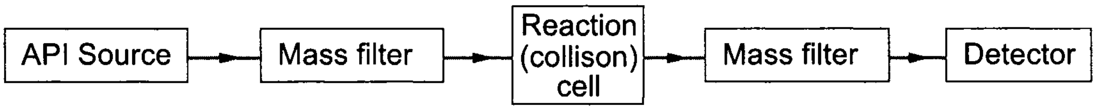

Figure 1.2 Schematic of a triple sequential mass spectrometer for biological studies.

In this arrangement, ions typically taken from an atmospheric pressure ion (API) source are delivered into a vacuum and subsequently injected into a preliminary mass filter set for a specific molecular mass. After this filter they are extracted and delivered to an ion guide where they are contained for sufficient periods of time to undergo chemical reactions with a selected background gas, or are excited to collide with background gas molecules at sufficient energy to fragment. The products are then delivered to yet another RFQ mass filter for mass analysis. The mass spectrum obtained is a very distinctive signature of the original selected molecules, allowing detection of trace quantities of such molecules in any biological sample in parts per billion.

While the RFQ ion confinement technique is very versatile, up to now it has only been used for relatively small numbers of ions and relatively weak beam currents. This is because of the mutual space charge repulsion of the contained ions, which the RFQ confinement must resist. The confinement forces that have been achievable in present devices can hold only beams of up to several nanoamperes and ion collections of up to only about one million. However, for mass measurements on many rare species the contaminants, which also must be handled by the capture system before sorting can be carried out, can produce beam currents many orders of magnitude more than this, sometimes up to microamperes. There is therefore a need for much stronger confinement fields to overcome the increased space charge forces of such beams.

Recent work, by the author [Gia02], has shown that, with proper care in the design and preparation of electrodes, very high RF fields can be sustained in a buffer gas at pressures approaching 100 Pa (one mbar). With the development of techniques for superimposing relatively small DC potentials on the very high RF potentials, high field RFQ confinement has become feasible. The present work is a first study of the use of high RFQ fields for ion confinement in a buffer gas.

There are many possible applications for the high field RFQ confinement of ions. In addition to the cooling of ion collections and delivery to a Penning trap mass measurement system, there is the possibility of cooling a continuous beam for subsequent extraction as a continuous beam with a significantly smaller emittance than the original. This would improve the transmission and resolution of sector magnet mass spectrometers, which still have wide application in physics, chemistry and biochemistry. It is also possible that the tighter confinement that could be achieved by high RFQ fields could render ions collections into a small enough phase space to enable high-resolution mass spectrometry by time-of-flight (TOF) methods. At present, commercial mass spectrometers using linear ion trap/time-of-flight configurations are capable of mass resolutions in the tens of thousand using femtomoles sized samples. Such systems extract the ions in a long, thin bunch and subsequently apply a sudden transverse field to direct them into a TOF spectrometer [Hop99] [Che99] [Lob03] [Dou05]. Unfortunately, such high performance TOF systems are very wasteful of the ionized sample having only a small fraction of the ions reach the detector. Tighter axial confinement using the high axial trapping fields that are possible with stronger RFQ confinement would greatly increase the sensitivity of mass spectrometry by allowing the direct delivery of the ions to the TOF spectrometer.

To enable the design of these possible uses for high field RFQ ion confinement the properties of the ions delivered from such confinement must be understood. In all of these the property of most significance is the phase space density of the collection. This is determined, essentially, by the temperature of the ion collection and the strength of the confining forces. This then is the subject of this thesis.

The vehicle for carrying out this study is a strong linear RFQ device, dubbed the HVTrap (High Voltage Trap). This trap has been designed specifically to probe the phase space density of ions collected in it by TOF detection of ions rapidly extracted from it. The resulting time profiles of the detected ion ensembles can then be fitted with computer simulated TOF signals where the individual parameters of the model can be adjusted until satisfactory fits to the data are achieved. This methodology closely follows the one used by Lunney [Lun92], Ghalambor-Dezfuli [Gha96] and Fong [Fon01], which has been shown to be quite successful in the study of the phase space distributions of ions in RFQ devices. As a result, more details on this methodology can be found in the references to their work.

1.1 Contributions of the Thesis

The main contributions of this thesis are proof that high-field RFQ confinement is feasible and the principles by which such confinement can be engineered for specific purposes, in particular as an ion source for high-resolution TOF mass spectrometry or for buffer gas cooling of intense ion beams at nuclear research facilities such as ISOLTRAP at CERN and TRIUMF in British Columbia. To bypass the electrical breakdown limits of modern electronic components, a novel voltage delivery scheme was developed to deliver the necessary RF and DC potentials to the trap electrodes to confine and manipulate charged particles within the RFQ system. Finally, to analyze the TOF signals of the ejected ion collections a SIMION simulation of the extraction process was developed to model the behavior of ejected ions and establish the equilibrium temperatures of the trapped ion ensembles.

Chapter 2 Theoretical Framework

Electrodynamic devices such as the quadrupole ion trap and quadrupole beam guide, both shown in figure 2.1, employ oscillating electric fields to confine and manipulate charged particles by accelerating them along electric field lines. While many different trapping schemes and electrode configurations have been developed over the years, the basic operating principles behind these devices have remained unchanged [Daw76].

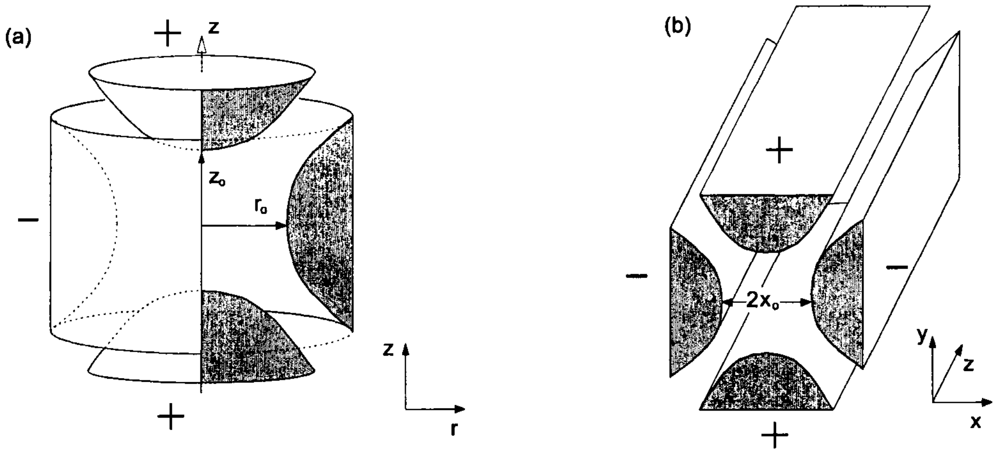

Figure 2.1 Two types of RFQ devices: a) quadrupole ion trap; b) quadrupole beam guide.

2.1 Ion Manipulation

The forces acting on particles of mass m and charge e within an electric field $\vec{E}$ are given by

$$\vec{F} = m\vec{a} = e\vec{E} \quad . \tag{2.1}$$

In the absence of charge centers Laplace's equation requires that

$$\nabla \cdot \vec{E} = 0 \tag{2.2}$$

which forbids the existence of a potential minimum in empty space. As a result, any field line entering such a volume will have to exit it as well, simultaneously creating a potential minimum in one direction and a potential maximum in an orthogonal dimension (see figure 2.2). This eliminates the use of electrostatic fields for the three dimensional confinement of charged particles. However, oscillating fields provide an elegant way around this difficulty. By inverting the electric fields after half a cycle and, consequently switching the potential maximum and minimum, charged particles can be made to experience a net confining force towards the trap center. For this to take place, however, appropriate oscillation frequencies need to be chosen which for ion confinement occurs in the radio frequency range.

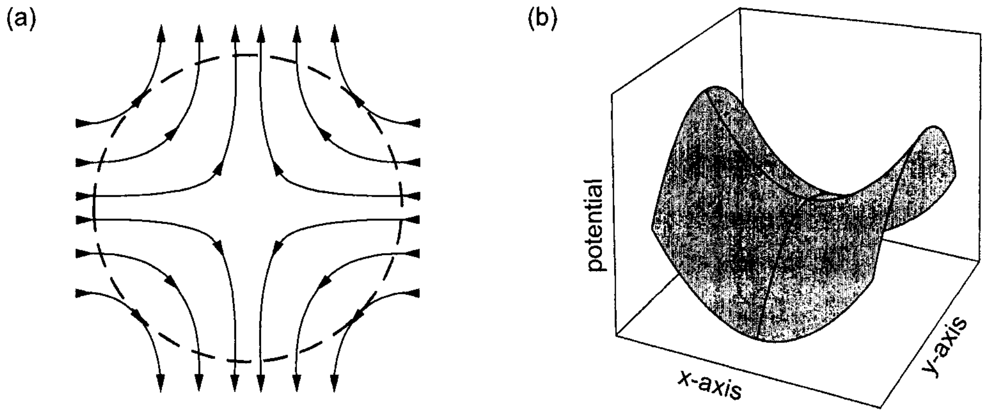

Figure 2.2 In the absence of charge centers, Laplace's equation forbids the existence of a potential minimum such that (a) field lines entering a volume must also exit it as well (b) creating a potential minimum in one direction and a potential maximum in the other.

Rewriting equation 2.2 in terms of electric potential gives us

$$\nabla^2\Phi = 0 \quad . \tag{2.3}$$

In spherical coordinates, general solutions to the above equation can be expressed as

$$\Phi = \sum_{lm} A_l^m \varphi_{lm} \tag{2.4}$$

where φ_{lm}, referred to as the electric multipole of the potential, is defined as

$$\varphi_{lm} = \rho^l P_l^m(\cos\theta)\cos m\phi \tag{2.5}$$

and $P_l^m(\cos\theta)$ are the associated Legendre polynomials. A_l^m, an arbitrary constant representing a given multipople's strength, is specific to a particular electrode configuration. For systems with axial symmetry along the z-axis, equation 2.4 then becomes

$$\Phi = \sum_{l=0}^{\infty} A_l^0 \rho^l P_l(\cos\theta) \tag{2.6}$$

Expanding the above series into its multipole constituents leads to a very interesting result. While both the first and second term in the expansion offer little or no possibility for ion confinement, the third term gives rise to an electric field that is proportional to the distance from the origin (i.e. the trap center). Known as the quadrupole field term, it allows ions to experience a restorative force towards the trap center which is proportional to their displacement from the origin and, as a result, allows them to undergo simple harmonic motion about the trap's center. Higher order terms such as the hexapole and octopole, on the other hand, exhibit non-linear behavior which leads to more complicated ion motion within the trap. While devices based on such higher order potentials are capable of ion confinement the non-linear behavior results in increased phase space volume, limiting their usefulness for ion cooling.

For linear devices such as the quadrupole beam guide shown in figure 2.1b), expressing the quadrupole potential in Cartesian coordinates offers a more suitable way of viewing the resulting ion motion within the trap. In Cartesian coordinates, the quadrupole field term becomes

$$\Phi = \Phi_o(\alpha x^2 + \beta y^2 + \gamma z^2) \tag{2.7}$$

However, in light of equation 2.3 we require that

$$\alpha + \beta + \gamma = 0 \quad . \tag{2.8}$$

For linear configurations where the *z*-axis is chosen as the beam axis and confinement fields are produced along the *x*-*y* plane

$$\alpha = -\beta \quad \text{and} \quad \gamma = 0 \quad . \tag{2.9}$$

The electric potential and resulting electric field then become

$$\Phi = \Phi_o \alpha (x^2 - y^2) \tag{2.10}$$

$$\begin{aligned} \vec{E} &= -\nabla\Phi \\ &= -2\Phi_o \alpha (x\mathbf{i} - y\mathbf{j}) \end{aligned} \quad . \tag{2.11}$$

The easiest way to create such quadrupolar fields is to manufacture four hyperbolic rods and place them along equipotential lines in the *x*-*y* plane (see figure 2.1b). If the minimum distance between opposing rods is $2r_{o,}$ equation 2.10 then becomes

$$\Phi = \frac{\Phi_o}{2r_o^2}(x^2 - y^2) \tag{2.12}$$

where Φ_o , the potential difference between neighboring rods, is

$$\Phi_o = U - V\cos\omega t \quad . \tag{2.13}$$

Inserting 2.12 and 2.13 back into 2.11 yields the complete oscillating quadrupole field

$$\vec{E} = \frac{-(U - V\cos\omega t)}{r_o^2}(x\mathbf{i} - y\mathbf{j}) \tag{2.14}$$

where *U* defines the DC component of the potential and *V* is the amplitude of the AC component.

Rewriting equation 2.1 in terms of the new electric potential given in (2.14), the equations of motion can now be expressed as

$$\begin{aligned}&\ddot{x}+\frac{e}{mr_o^2}(U-V\cos\omega t)x=0\\&\ddot{y}-\frac{e}{mr_o^2}(U-V\cos\omega t)y=0\end{aligned}\quad, \tag{2.15}$$

allowing another key feature of the quadrupole field to emerge: while the overall trajectory of the confined particles can be a jumbled mess, the motion can be decoupled and analyzed independently in each dimension. Rearranging and redefining some of the terms in (2.15), we obtain the canonical form of the Mathieu equation

$$\frac{d^2u}{d\xi^2}+(a_u-2q_u\cos 2\xi)u=0 \tag{2.16}$$

where

$$a_u=a_x=-a_y=\frac{4eU}{m\omega^2 r_o^2} \tag{2.17}$$

$$q_u=q_x=-q_y=\frac{2eV}{m\omega^2 r_o^2} \tag{2.18}$$

$$\xi=\frac{\omega t}{2}\quad. \tag{2.19}$$

Solutions to equation 2.16 have the general form

$$u=\alpha' e^{\mu\xi}\sum_{n=-\infty}^{\infty} C_{2n}\, e^{2in\xi}+\alpha''\, e^{-\mu\xi}\sum_{n=-\infty}^{\infty} C_{2n}\, e^{-2in\xi} \tag{2.20}$$

where α' and α'' are integration constants related to a particle's initial conditions and the constants C_{2n} and μ depend on the stability parameters a and q. Stable solutions to equation 2.20, when μ remains finite as $\xi\to\infty$, result in stable ion trajectories (i.e. confinement) within the quadrupole device. These stable solutions occur when μ is purely imaginary such that $\mu=i\beta$ and β is not an integer. Given that μ is only dependent on the values of a and q, the stability conditions can be represented by a-q diagrams such as the one shown in figure 2.3 where typical values for linear trap configurations are $0 \le \beta \le 1$.

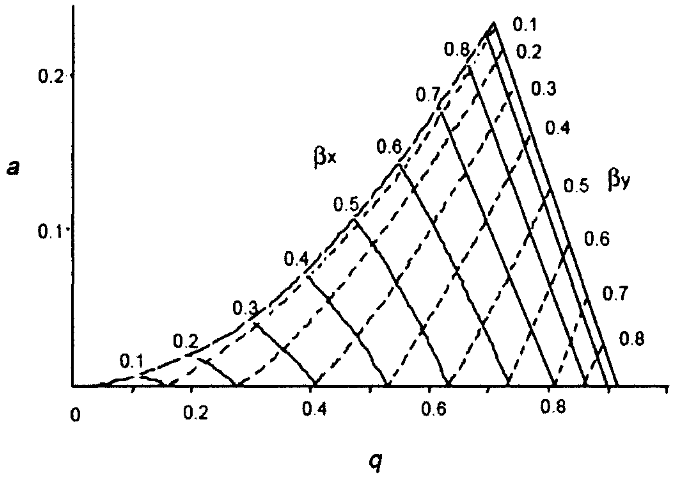

Figure 2.3 **Stability diagram for linear ion traps.**

Stable ion trajectories within RFQ devices are characterized by fundamental *macromotion* oscillations with higher frequency oscillations, referred to as *RF motion*, superimposed onto it (see figure 2.4). While the RF motion is tied to the quadrupole's driving frequency, the macromotion oscillation is best understood as a particle's motion within the *pseudopotential* well created by the device's quadrupole fields. For small values of β such that $\beta \le 0.4$, the relationship between macromotion and RF motion can be approximated by

$$\omega_M = \frac{\beta\omega}{2} \cong \frac{q}{2\sqrt{2}}\omega \tag{2.21}$$

while the pseudopotential well depth, which is indicative of the strength of confinement, is given by

$$D_{pseudo} = \frac{1}{2} m \omega_M^2 r_0^2 \tag{2.22}$$

To increase the well depth, and consequently the strength of confinement, it follows from equation 2.22 that one would have to either increase the electrode separation r_0 or increase the macromotion frequency ω_M. Increasing r_0 is easily accomplished by making the trap larger whereas increasing ω_M can be accomplished by either increasing the field gradient across the RFQ or by decreasing the RF driving frequency at a given potential (see equations 2.18 and 2.21).

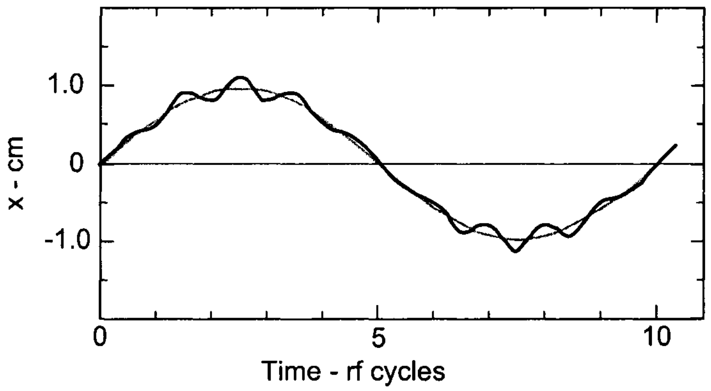

Figure 2.4 Typical motion of a charge particle in an oscillating electric field where the RF motion is proportional to the distance from the trap center.

While decreasing the driving frequency may be beneficial for very low values of q, at higher values the addition of the RF motion to the macromotion can result in a considerable reduction of the usable trapping volume. In fact, at values of q approaching unity, the RF motion becomes so violent that ion trajectories become unstable and confinement ceases (see figure 2.5). Increasing r_0 also has its limitation since trapping systems cannot be enlarged indefinitely. As a result, increasing field gradients across the RFQ traps becomes the only viable choice to increasing the confinement strength of quadrupole devices.

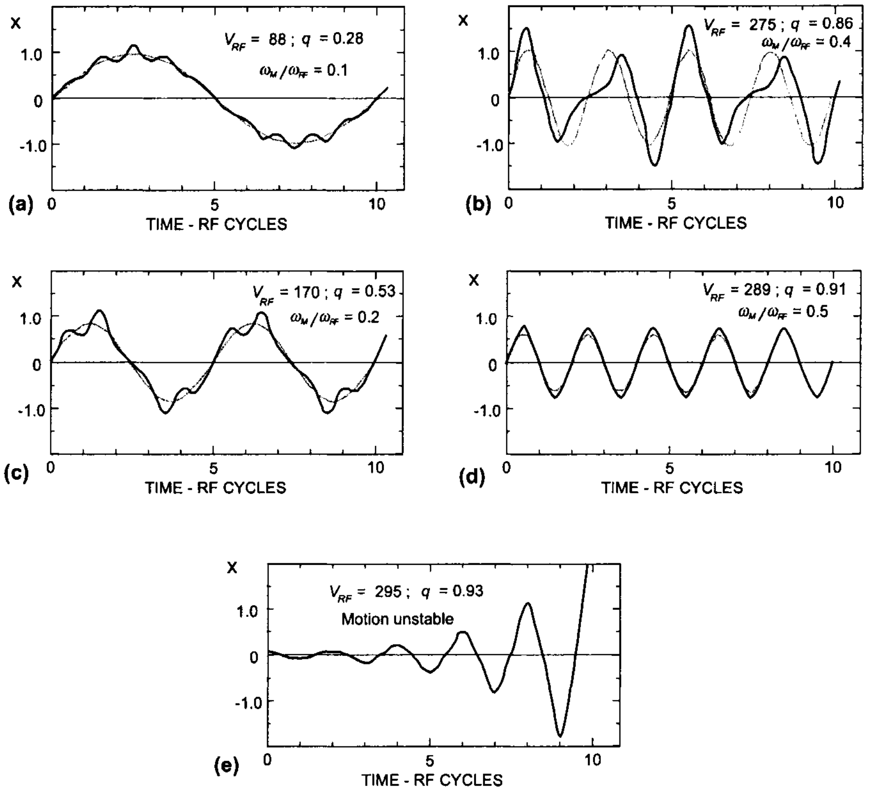

Figure 2.5 **Particle motion in an oscillating electric field at various values of *q*. Beyond *q* values of 0.91, trajectories are unstable and particles are no longer confined (see graph e).**

2.2 Phase Space Dynamics

Although motion in a quadrupole field is inherently independent in each direction and sufficiently approximated by the simple harmonic oscillator model described above, a particle's overall trajectory can still seem like a very complex and tangled mess (see figure 2.6). Consequently, keeping track of the individual trajectories for a collection of particles quickly becomes a daunting task. By projecting each particle's position coordinates (x,y,z) and momentum coordinates (p_x, p_y, p_z) at a given moment into the corresponding 6 dimensional phase space, one can very easily visualize the time evolution of the original collection.

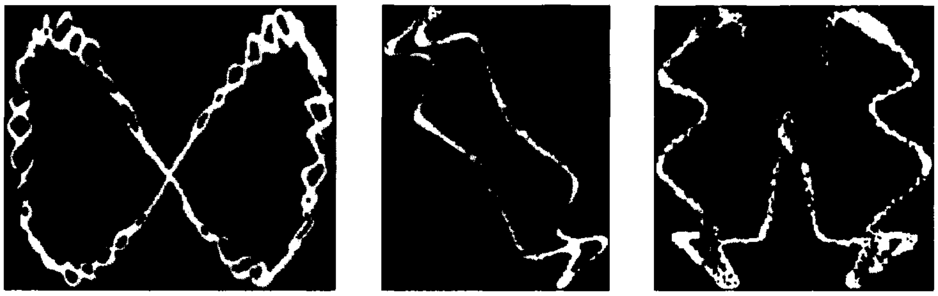

Figure 2.6 Actual trajectories of trapped aluminum micro-particles [Daw76].

In the absence of non conservative forces and particle interactions, Hamiltonian mechanics describes the total energy H of a collection of particles in a RFQ field as

$$H = \sum_{i=1}^{n} \frac{p_i^2}{2m} + \frac{kq_i^2}{2} \tag{2.23}$$

where the canonical form of the generalized position q_i and generalized momentum p_i are given by

$$\dot{q}_i = \frac{\partial H}{\partial p_i} = \frac{p_i}{m} \tag{2.24}$$

$$\dot{p}_i = -\frac{\partial H}{\partial q_i} = -kq_i \quad . \tag{2.25}$$

Solutions to the above equations take the form of those for a simple harmonic oscillator where

$$q_i = A_i \cos(\omega t + \phi) \tag{2.26}$$

$$p_i = -A_i m\omega \sin(\omega t + \phi) \quad . \tag{2.27}$$

In phase space, these solutions are represented by a family of ellipses in each dimension (figure 2.7) where A_i represents the maximum amplitude of oscillation of the i^{th} particle and $\omega = \sqrt{k/m}$. Furthermore, the unique nature of these solutions for a given set of initial conditions prevents any two elliptical paths from intersecting one another.

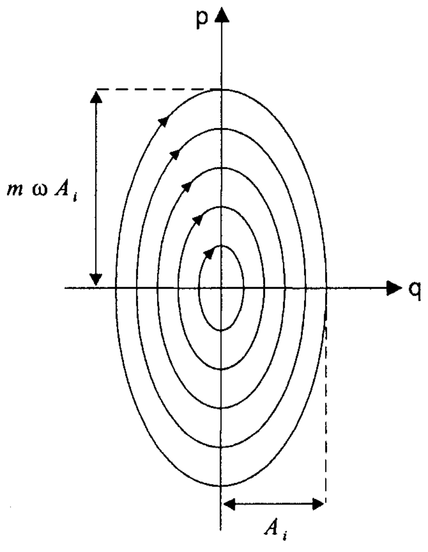

Figure 2.7 Phase space ellipses representing the paths of confined particles.

Since each particle corresponds to a point in phase space, a collection of particles would therefore be represented by a cloud of points in the phase space volume S defined as

$$S = S_X S_Y S_Z = \int dx dp_x \int dy dp_y \int dz dp_z \tag{2.28}$$

where the phase space areas S_x, S_y and S_z, also known as action areas, are projections of the total phase space volume in each dimension. As a result, the number of points dN in an infinitesimal volume dS will remain constant as the particle ensemble evolves in time. Accordingly, the ensemble's phase space density $D = dN/dS$ will also remain constant. Known as Liouville's theorem, this result is best understood by comparing a collection of particles in phase space to an uncompressible gas (see figure 2.8). While the surface surrounding the group of particles may change shape over time, the density of particles within the surface will remain constant [Law83]. Moreover, given the uncoupled nature of a confined particle's motion in a quadrupole field, each phase space area will also behave as an "uncompressible gas" allowing one to follow the time evolution of the particle ensemble independently in each dimension.

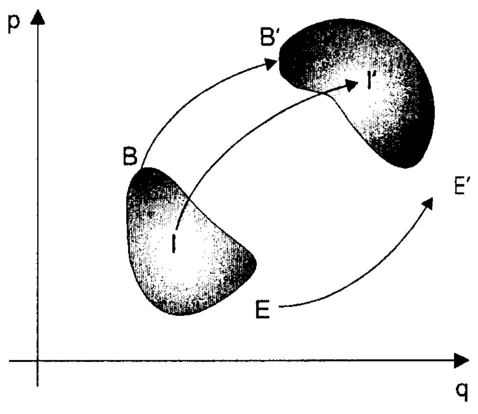

Figure 2.8 **Liouville's theorem shows that as a phase space volume changes shape over time (B becomes B') the interior points remain within the volume (I=I') while the exterior points remain outside (E=E').**

When dealing with a collection of particles, it is sometimes more practical to represent the entire system by boundary ellipses in each action area corresponding to the outermost path capable of being taken by a particle within the given ensemble. These boundary ellipses, shown in figure 2.9, can then be written as

$$\gamma q^2 + 2\alpha qp + \beta p^2 = \varepsilon \tag{2.29}$$

where

$$\varepsilon = \frac{\text{area of the ellipse}}{\pi} \tag{2.30}$$

and

$$\tan 2\theta = \frac{-2\alpha}{\beta - \gamma} \tag{2.31}$$

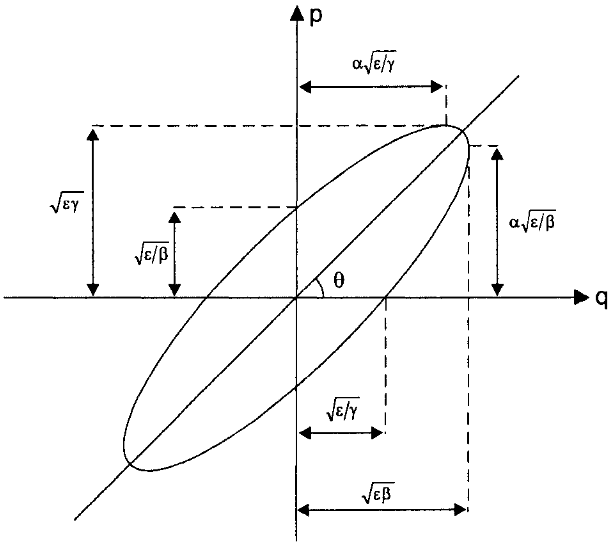

Figure 2.9 Critical values of a boundary ellipse in a given action diagram.

In beam transport systems, boundary ellipses correspond to limiting values of position and momentum that a particular system can accept or transmit a set of particles. By perfectly matching the acceptance and emittance between two systems, one can transport a collection of particles undisturbed. Any discrepancy between the two, however, will inevitably lead to a loss of particles during transport (figure 2.10).

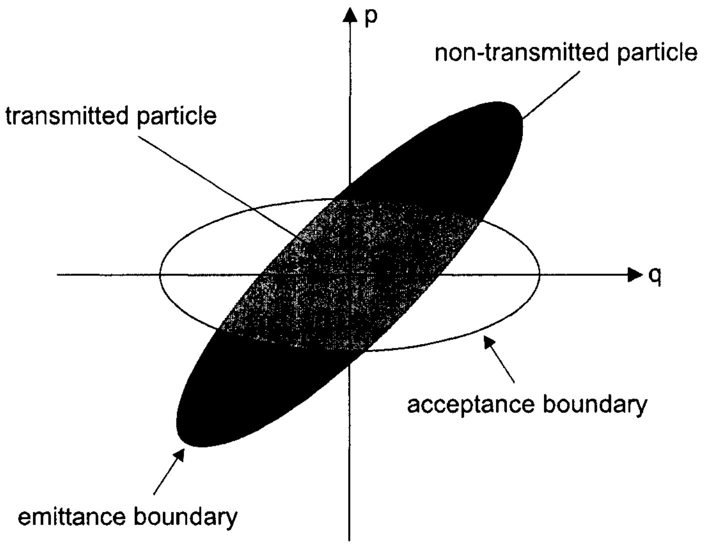

Figure 2.10 Acceptance/Emittance ellipses.

In field free regions, where the particles experience no external forces, the time evolution of each particle is given by

$$q(t) = q_{\text{int}} + \frac{p_{\text{int}}}{m}t \qquad p(t) = p_{\text{int}} \tag{2.32}$$

where q_{int} and p_{int} are the initial position and momentum coordinates at $t=0$. As time progresses the original configuration is gradually skewed as the position coordinates increase proportionally with Δp and the momentum spread remains the same in the absence of external forces (see figure 2.11).

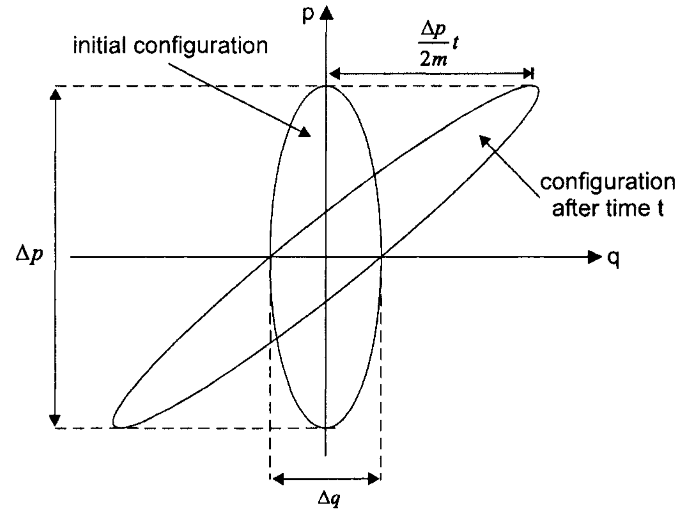

Figure 2.11 **Time evolution of a set of particles in a field free region.**

In the presence of a uniform electric field E, however, both spatial and momentum spreads will change after a time t as the particle ensemble experiences a force $F = eE$ in the $+q$ direction (figure 2.12). In this situation

$$q(t) = q_{\text{int}} + \frac{p_{\text{int}}}{m}t + \frac{eE}{2m}t^2 \qquad p(t) = p_{\text{int}} + eEt \tag{2.33}$$

resulting in a shift of the ensemble center given by

$$\begin{aligned} dq &= eEt^2/2m \\ dp &= eEt \end{aligned} \tag{2.34}$$

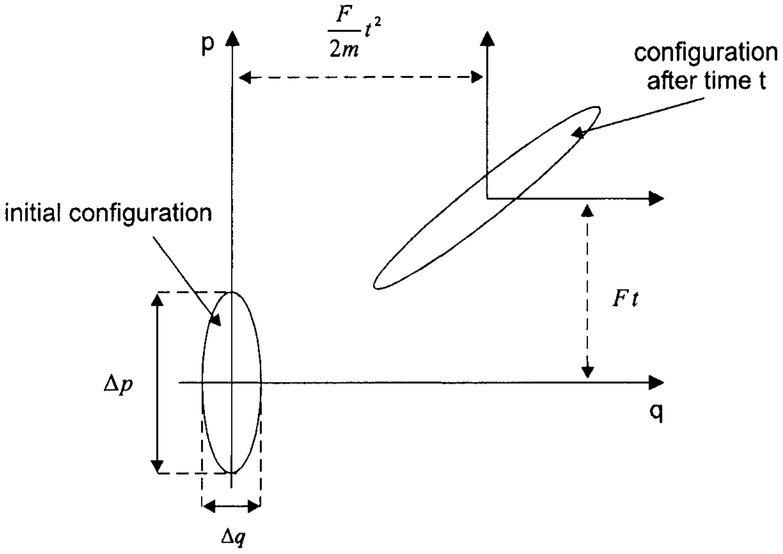

Figure 2.12 Time evolution of a set of particles traveling in a constant field free region.

2.3 Ion Temperature

Although it is possible to fully characterize and follow the evolution of large particle ensembles in phase space, macroscopic quantities such as spatial distributions and velocity distributions are best handled using statistical mechanics. Inevitably, this statistical mechanics approach to ion trapping leads to the definition of an ensemble's temperature governing both the spatial and velocity distributions in a given phase space volume.

Beginning with the Gibb's distribution, the number of particles N occupying a phase space volume S can be given by

$$\frac{d^6N}{dS} = C\,e^{\frac{-E}{k_BT}} \tag{2.35}$$

where T is the system's temperature and k_B, the Boltzmann constant, is defined as $k_B = 8.617\times10^{-5} eV/K$. If the ensemble has reached an equilibrium state between the trapping potentials and space charge repulsion caused by the ions within the ensemble and the pseudopotential well model sufficiently describes the system, the total energy E can be given by

$$E=\sum_{i=1}^{n}\frac{p_i^{\,2}}{2m}+\frac{1}{2}m\omega^2 q_i^{\,2} \tag{2.36}$$

Since each canonical pair of coordinates can be dealt with separately in light of the decoupled nature of an ion's motion in quadrupole fields, the density distribution can then be rewritten as

$$\frac{d^2N}{dq_i dp_i}=\frac{N_o\omega}{2\pi k_BT}e^{-\frac{m\omega^2}{2k_BT}\left(q^2+\left(\frac{p}{m\omega}\right)^2\right)} \tag{2.37}$$

where N_0 is the total number of particles in the ensemble. Integrating over dq_i from $-\infty$ to ∞ results in

$$\frac{dN}{dp_i}=\frac{N_o}{\sqrt{2\pi mk_BT}}e^{\frac{-p^2}{2mk_BT}} \tag{2.38}$$

while integrating over dp_i from $-\infty$ to ∞ yields

$$\frac{dN}{dq_i}=N_o\sqrt{\frac{m\omega^2}{2\pi k_BT}}e^{\frac{-m\omega^2q^2}{2k_BT}} \tag{2.39}$$

As can be seen from equations 2.38 and 2.39, both position and momentum distributions are Gaussian in nature with standard deviations σ_{q_i} and σ_{p_i} given by

$$\sigma_{q_i}=\frac{1}{\omega}\sqrt{\frac{k_BT}{m}}\quad,\qquad \sigma_{p_i}=\sqrt{mk_BT} \tag{2.40}$$

Translating this into boundary ellipses in a 2 dimensional phase space results in 40% of the particle ensemble laying within a 1σ radius of the ensemble's center, 87% contained within a 2σ radius and 99% of the ensemble found within a 3σ radius (see figure 2.13).

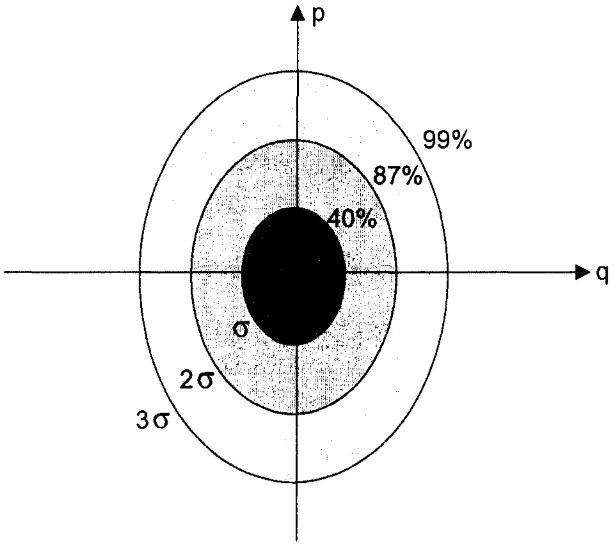

Figure 2.13 The density distribution of a collection of particle in a SHO at thermal equilibrium.

Although the above equations presuppose an equilibrium state between the ion ensemble and the trapping environment, a number of mechanisms have been found to play a key role in the rate at which this equilibrium state can be reached as well as the ensemble's final equilibrium temperature.

By introducing a light, neutral background gas into the trapping environment a viscous drag effect is created between the confined ions (m_i) and the background gas molecules (m_n) [Deh67] [Maj68]. When $m_i > m_n$, many soft collisions between the heavier ions and the light background gas produce small fractional losses of the ions' kinetic energy resulting in a reduction of the ensemble's overall energy and a cooling of the confined particles[†]. Known as collisional cooling (or buffer gas cooling), the equation of motion of an ion under viscous drag in a quadrupole field becomes

$$m_i\ddot{x} + \frac{e}{K}\dot{x} = e\frac{dE_{Field}}{dx}x\sin(\omega t) \tag{2.41}$$

where K is the ion mobility constant. When the ion velocities are low compared to the thermal velocities of the buffer gas, K is defined as

$$K = v/E_{Field} \tag{2.42}$$

i.e., the ratio between the ion's terminal velocity v within the gas and the electric field E_{Field}. Since ion mobility is inversely proportional to the collision rate with the background gas molecules, it will also be inversely proportional to the buffer gas pressure. Consequently, the damping term introduced by the gas viscosity exponentially reduces the amplitude an ion's motion within a RFQ trap. For large values of K the viscosity term is insignificant and the motion is just the simple harmonic macromotion. For small values of K, however, the macromotion oscillation diminishes proportionally to the gas pressure until critical damping is reached. Beyond critical damping, it becomes progressively harder to force the ions to the center of the quadrupole field as more buffer gas is introduced into the RFQ system. The decay rate of the overall motion then becomes inversely proportional to the cube of the buffer gas pressure (see figure 2.14).

It should be noted, however, that the above development is only valid for ion velocities that are comparable to the thermal velocities of the buffer gas molecules. When the ion velocities are much greater than that of the gas molecules, which is usually the case, collision rates between the ions and the gas molecules become proportional to the ion velocities. This results in the viscous drag forces increasing proportionally with the square of the velocity and the inverse of the ion mobility increasing linearly with the ion's velocity (see in figure 2.15).

[†] Note: the use of heavier background gas such that $m_i \leq m_n$ results in a general increase of the ion ensemble's kinetic energy followed by a loss of particle confinement.

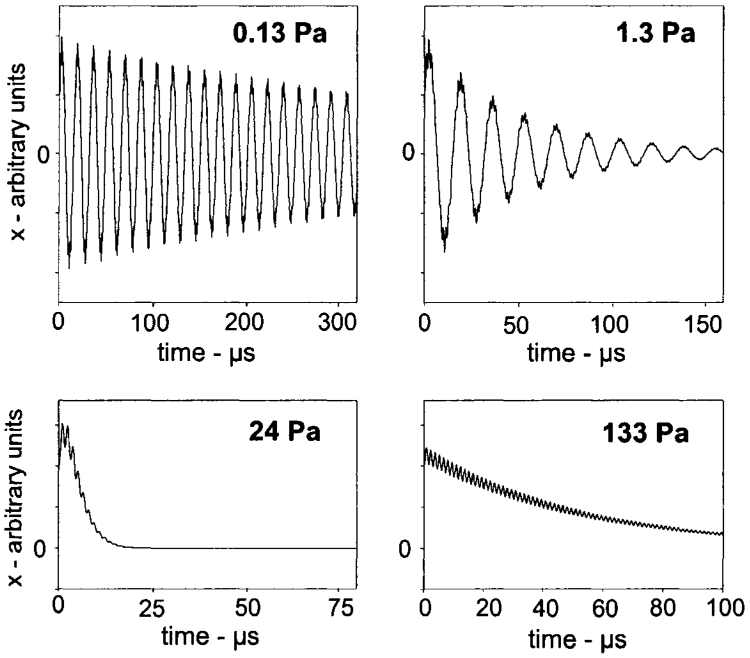

Figure 2.14 Damped motion of a Cs$^+$ ion in a RFQ field in a background of nitrogen at various pressures. The pressure for critical damping at the given confinement parameters was about 5 Pa.

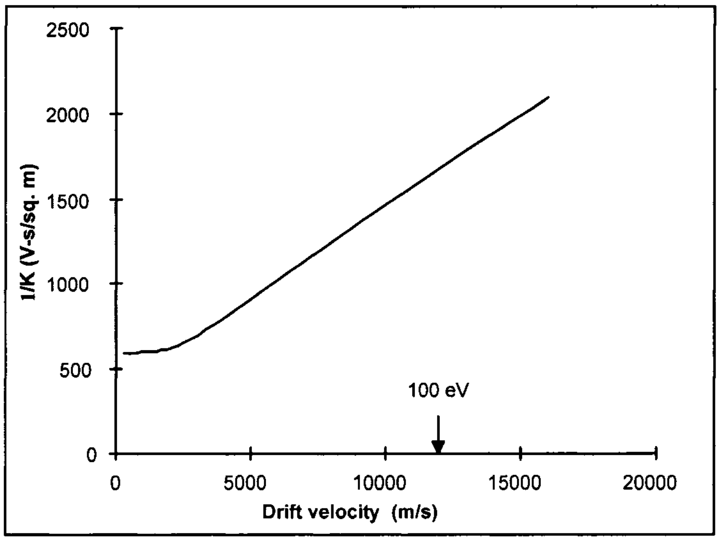

Figure 2.15 Mobility of Cs$^+$ in helium buffer gas at high velocities. Mobility data was graphed up to velocities of about 5000 m/s and extrapolated to higher velocities by theoretical values calculated from the known collision cross-sections of Cs$^+$ ions on helium molecules [Vie75].

In real systems, RF motion also plays an important part in determining the ensemble's equilibrium temperature. While the RF motion itself is a coherent movement and does not play a direct role in the statistical distributions associated with an ensemble's temperature, collisions between the coherent RF motion of the ions and the background gas can lead to incoherent motion within a particle collection that inevitably increases the ensemble's overall temperature. Known as RF heating, the RF micromotion caused by the trap's driving frequency is immediately replaced after each collision by the RF field leading to a continuous heating process within the trap. Under certain circumstances, this heating can cause an ion ensemble to become greater than the actual size of the trapping region leading the outermost ions of the ensemble (i.e. the more energetic particles) to collide with the trap electrodes and be removed from the collection. This removal process, known as evaporative cooling, continues until the ion ensemble is no longer restricted by the physical trapping system and results in gradual cooling of the entire particle ensemble.

While lengthy Monte-Carlo simulations [Kim97] have had some success in treating these heating processes, the most generally useful results have come from the works of Lunney [Lun92] and Kim [Kim97] who obtained measurements of the macromotion temperatures in RFQ devices. In both cases, the ensemble's temperature was dependent on the number of confined ions which was attributed to the space charge repulsion within the ensemble forcing ions out of the center of the trap into higher RF fields. This then led to greater heating of the entire ensemble. For the case of the Paul trap, where the space charge field is dispersed into three dimensions, the increase in temperature for small numbers of ions was found to be proportional to the 2/3rd power of the ion number. For the particular operating conditions chosen in the work of Lunney, the proportionality constant was estimated to be of the order of

$$\Delta T_{eV} \sim 5 \times 10^{-9} N^{\frac{2}{3}} \tag{2.43}$$

For the ion guide case, on the other hand, where the electric field of the collected charge is dispersed only in the radial direction from the axis, the increase in temperature for small numbers of ions was found to be proportional to the ion number. For the particular operating conditions chosen in the work of Kim, the proportionality constant was of the order

$$\Delta T_{eV} \approx 5\times10^{-10}\left[\frac{N}{\ell}\right]_{m^{-1}} \qquad (2.44)$$

where N/ℓ is the ion number per unit length of the guide.

2.4 Space Charge Limits

In order to estimate the possible effects of space charge repulsion within a confined ion ensemble, it is important to determine a given RFQ's space charge limit. For a very long cylinder of charge of radius r, the radial electric field at the surface can be expressed by

$$E_r = \frac{1}{2\pi\varepsilon_0}\frac{Q'}{r} \qquad (2.45)$$

where Q' is the charge per unit length of the cylinder. If the charge is confined to this radius by a quadrupole field given by

$$E_{confining} = -k\,r \quad . \qquad (2.46)$$

The linear charge density then becomes

$$Q' = 2\pi\varepsilon_0 k\,r^2 \quad . \qquad (2.47)$$

The volume charge density Q''' is therefore uniform and is given by

$$Q''' = 2\varepsilon_0 k \qquad (2.48)$$

The RFQ confinement of charged particles of mass m and charge e is equivalent to a radial electric field of

$$E_{RFQ\,confinement} = -\frac{m}{e}\omega_M^2\, r \tag{2.49}$$

where ω_M is the macromotion angular frequency of the confined ions. The density of the confined charge is then given by

$$Q''' = 2\varepsilon_0 \frac{m}{e}\omega^2 \quad , \quad Q' = 2\pi\varepsilon_0 \frac{m}{e}\omega^2 \mathrm{r}^2 \tag{2.50}$$

If the charge collection is held in a long linear trap then (2.51) leads to

$$r^2 = \frac{e\,Q'}{2\pi\varepsilon_0 m}\frac{1}{\omega^2} \tag{2.51}$$

If the linear charge density is expressed in number of singly-charged particles per mm, the mass of the charged particles in atomic mass units (amu), and the angular frequency in radians per microsecond, then the radius in mm due to the macromotion only is given by

$$r_{mm}^2 = 2.78\times10^{-4}\,\frac{n_{/\,mm}}{m_{amu}\,\omega_{rad\,/\,\mu s}^2} \tag{2.52}$$

while the radius including the micromotion is approximated by

$$r_{mm}^2 = 5.6\times10^{-5}\left(1+\frac{q}{2}\right)^2 \frac{n_{/\,mm}}{q^2 m_{amu} RF_{MHz}^2}\,. \tag{2.53}$$

The confinement of ions in a trap, however, must also include an axial electric field term to overcome the axial space-charge repulsion. The required field is easiest to calculate when the ion collection is of uniform density along a length that is much greater than its radius and the field is applied only at the ends of the collection. The electric field at the end of the collection due to the space charge of the whole collection can then be obtained by integrating the field over the collection volume. The first integration is that for the rings of charge making up a disk of thickness *dz* at distance *z* from the end of the collection (figure 2.16).

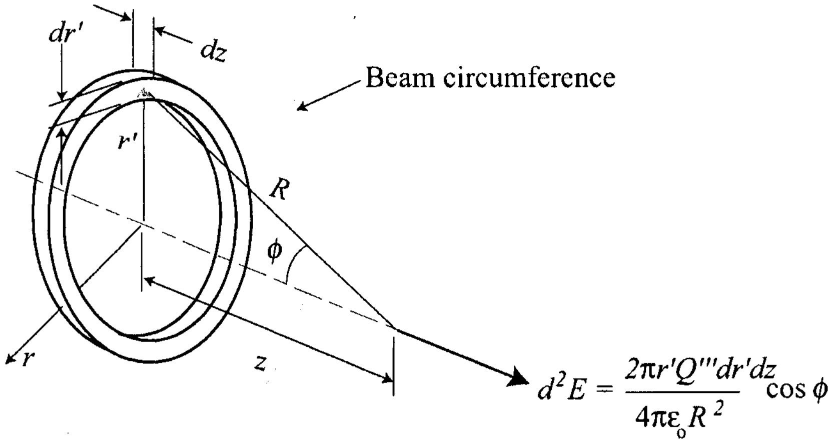

Figure 2.16 Integration cross section.

This integration has the form

$$dE = \frac{Q''' \, dz}{2\varepsilon_o} \int_0^r \frac{r'}{R^2} \cos\phi \, dr' \tag{2.54}$$

Substituting $r' = R\sin\phi$ and $dr' = \frac{R}{\cos\phi} d\phi$ results in

$$dE = \frac{Q''' \, dz}{2\varepsilon_o} \int_0^{\phi_b = \tan^{-1}\frac{r}{z}} \sin\phi \, d\phi = \frac{Q'''}{2\varepsilon_o} \left(1 - \cos\phi_b\right) dz \tag{2.55}$$

The electric field at the end of the charge column at $z = 0$ is the integration of the electric field from these disks over z from minus infinity to zero;

$$E = \frac{Q'''}{2\varepsilon_0} \int_{-\infty}^{0} (1 - \cos\phi_b)\, dz \tag{2.56}$$

From $dz = \frac{r}{\sin^2\phi_b} d\phi_b$

$$E = \frac{Q''' r}{2\varepsilon_0} \int_0^{\frac{\pi}{2}} \frac{(1 - \cos\phi_b)}{\sin^2\phi_b} d\phi_b = \frac{Q''' r}{2\varepsilon_0} \frac{(-\cos\phi_b + 1)}{\sin\phi_b} \quad (\phi_b = 0 \text{ to } \frac{\pi}{2}) \tag{2.57}$$

$$E = \frac{Q''' r}{2\varepsilon_0} \tag{2.58}$$

In terms of the linear charge density Q' the electric field is

$$E = \frac{Q'}{2\pi\varepsilon_0} \frac{1}{r} \tag{2.59}$$

If the linear charge density is expressed in singly-charged particles per mm $n'_{/mm}$ and the collection radius in mm the electric field at the ends of the collection can then be given by

$$E_{V/mm} = 2.9 \times 10^{-6} \frac{n'_{/mm}}{r_{mm}} \tag{2.60}$$

2.5 Time-of-Flight Spectrometry

As stated in the introduction, the method used to probe the phase space volume of a collection of ions under high-field RFQ confinement is TOF spectrometry. Here the rate of arrival of ions as a function of time after the application of an extraction pulse is used to deduce the phase space structure of the collection while it was in the trap.

TOF spectrometry is based on the behaviour of the axial action diagram of particles between the application of the extracting electric field and the arrival of the collection at the time of flight detector. To understand this, consider a collection of ions of 100 amu that have suddenly been produced, as by a short laser pulse in a gas, as a collection that, as shown in the diagram of the left of figure 2.17, has an axial extent of 1 mm and a kinetic energy up to that which corresponds to a momentum of 2.0 eV-μs/mm. The axial action diagram for this collection is shown in the diagram of the right of the figure.

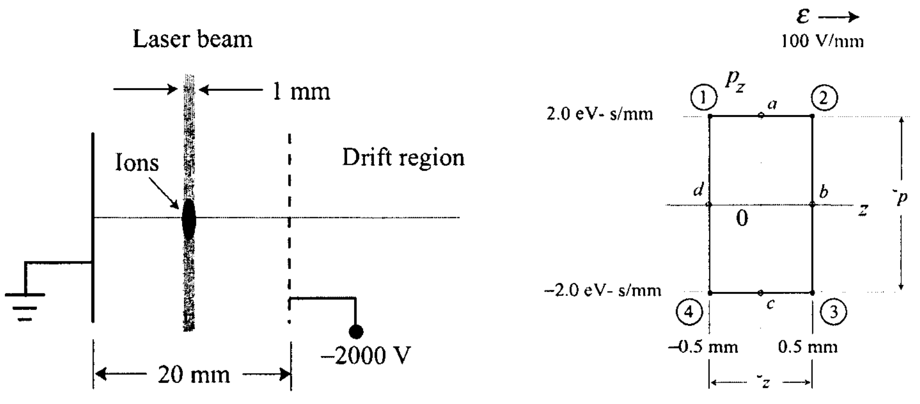

Figure 2.17 The spatial diagram and the axial action diagram of a collection of ions at the moment of production by a sharp laser pulse in a high electric field.

Now consider the axial action diagram at the exit of the field region. This is shown in figure 2.18. In this diagram the coordinates are energy and time, in accordance with the desire to know the time behaviour of the collection. Here the labels in circles indicate the corners of the action diagram as labeled in figure 2.17.

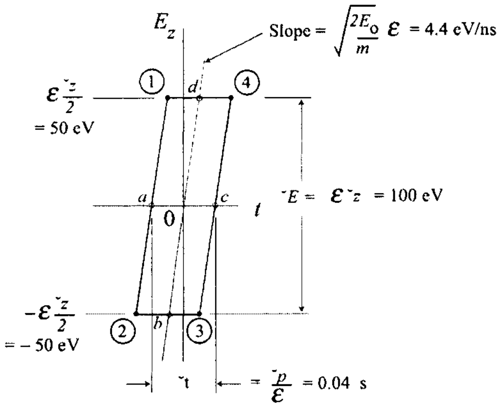

Figure 2.18 The axial action diagram of the particles in figure 2.17 as they enter the field free drift region. The central energy of this collection, i.e. the origin, is 1000eV.

Although the diagram appears to be a parallelogram, its almost vertical sides are actually slightly curved. They would only be perfectly straight in the extreme of the final extraction energy, in this case 1000 eV being much greater than the initial kinetic energy of the ions at production. In any case, it is seen that the action area is the same in both the initial action diagram and the diagram at extraction, i.e., 4.0 eV-μs.

Because the higher energy particles arrive earlier downstream, i.e., move to the left in the *E-t* action diagram, after a short drift, in fact of 20 mm, the action diagram of figure 2.18 will become a rectangle. However, after that the action diagram stretches out into a long parallelogram, as shown in figure 2.19.

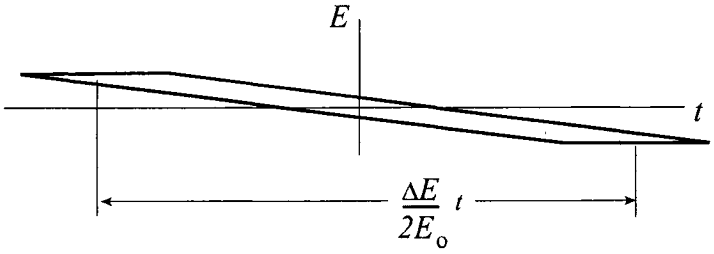

Figure 2.19 The axial action diagram of the particles in figure 2.18 after a long drift.

It is this diagram that is to be sampled by the TOF detector in the present work, where it will, essentially, take vertical slices along the extent of the diagram to determine the ion content of each slice. Here it is important to note that this sampling of the action diagram determines the distribution of the ions along the momentum axis in the original action diagram before the ions were extracted. Assuming the ion collection to be in thermal equilibrium, this momentum distribution of the ions is directly related to the temperature of the collection.

2.6 Time-of-Flight Mass Spectrometry

From figure 2.19 it can be seen that a collection of ions having all the same mass will have quite a spread in their arrival times at a detector just due to their original momentum spread. However, this spread can be considerably reduced by time-focusing the collection so that the axial action diagram at the detector is again a rectangle. This can be done by using a "reflectron" which reverses the paths of the ions. The resulting transformation of the axial action diagram is shown in figure 2.20.

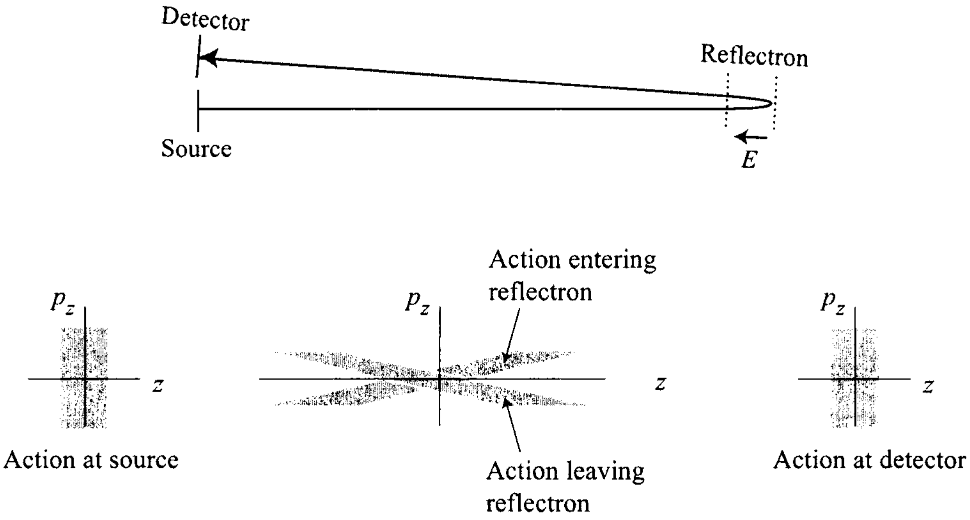

Figure 2.20 A schematic of a reflectron and it influence on the axial action diagram of ions entering it.

Simply, in this device the high energy ions, that enter first, go deeper into the reflecting electric field, thereby losing ground to the lower energy ions that come later but do not go so deep. The result is a flip of the action diagram so that it now drifts to a time focus, i.e. a rectangle. This minimizes the time spread for a given ion to the width of the action diagram. Since the action area is an invariant property of the ion collection that is determined by its temperature and confinement parameters, equation (2.40), the time spread at a detector is this action area A_z divided by the axial energy spread at detection;

$$\Delta t = \frac{A_z}{\Delta E} \tag{2.61}$$

Since the resolution of the spectrometer is determined by how narrow a time window the ions of a specific type will arrive in, we have the counterintuitive result that a larger energy spread in the extracted ion collection will result in better mass resolution. A little manipulation of the equations shows that the actual mass resolution is related to the axial action area as

$$R \equiv \frac{m}{\Delta m} = \frac{1}{2}\frac{t}{\Delta t} = \frac{1}{2}\frac{t\,\Delta \mathrm{E}}{A_z} \tag{2.62}$$

where t is the overall drift time in the TOF apparatus. Since a high-field RFQ linear trap keeps a collection of ions in a small phase space, providing the temperature of the ions is not excessive, it could be very interesting as a possible source for a TOF mass spectrometer.

2.7 Electrical Breakdown

In designing and building a high-field RFQ device, the possibility of electrical breakdown must be taken onto account. The following is a selection of material dealing with this problem for the scale of instrument that had to be built for the present work.

Although microscopic protrusions on electrode surfaces are known to play a significant role in vacuum breakdowns [Cha67] it is very difficult to control the microscopic profile of these surfaces. Certain macroscopic parameters, however, can be adjusted in order to improve the breakdown potential between a set of electrodes. The most obvious and perhaps hardest parameter to quantify is the electrode separation. It is the hardest to quantify because it depends on a large number of factors such as electrode configuration, breakdown history and environment. In some cases, factors such as electrode polishing are ill defined and difficult to reproduce. For DC voltage sources, the general rule to emerge is that for small gaps ($d \leq 0.5$mm) the breakdown voltage V_b is given by

$$V_b = E_b d \tag{2.63}$$

where E_b is the electric field at breakdown. At these gap spacings it is generally believed that field emission processes govern the breakdown mechanism and E_b is generally in the range of 6-8x10^7 V/m for optimal experimental conditions. For large gaps, where $d \geq$ 2mm, it is believed that microparticles dominate the breakdown process and V_b can be approximated by

$$V_b = kd^{\alpha} \tag{2.64}$$

where k varies between 40-45 kV/mm$^{-\alpha}$ and α is between 0.4-0.6. In the transition range 0.5mm $\leq d \leq$ 2mm, it becomes increasingly hard to establish a general behavior for the breakdown voltage since both field emission and microparticle processes develop simultaneously and can interact with each other.

Electrode materials also play a crucial role in the breakdown development. It has been well documented that materials such as copper and nickel produce unstable electrodes while stainless steel and titanium have become to some extent the high-voltage engineering standard. Aside from being hard metals, which might offer some degree of protection against surface defects potentially caused by microparticle impacts, they also have a thin strong insulating ambient oxide film protecting them against corrosion. This makes them very well suited for vacuum environments since a thick layer of oxidation on the surface can outgas, thereby providing an ionizable medium for electrical breakdown to occur.

The presence of certain foreign gas species has also been known to significantly improve the breakdown potential between electrodes. This is particularly true for inert gases such as N_2, He and SF_6. It is believed that chemisorption and physi-sorption processes at the electrode surfaces actually raise the surface work function ϕ of the metallic electrode therefore lowering the γ factor of microprotrusions due to decreases in current densities at protrusion tips. This, in turn, reduces any sputtering that may occur at the electrode surface diminishing the amount of electrode material released within the electrode gap.

Another parameter, which can also have profound impact on the breakdown potential of a particular system, is the waveform of the voltage. In the case of sinusoidal waveforms, observations have shown slight difference between peak AC breakdown voltages and peak DC voltages. In general, AC voltages are about 10% higher than DC breakdown voltages and have been shown to be independent of frequency up to 250 Hz. Results have also shown a clear transition point between large gap and small gap voltage breakdowns V_b. Empirically, the AC breakdown voltage V_b for small gap spacings ($0.05 \leq d \leq 1.5$mm) is given by

$$(V_b)_{ac} = 45d^{0.85} \tag{2.65}$$

while for larger gaps ($1.5 \leq d \leq 2.8$mm), V_b follows

$$(V_b)_{ac} = 57d^{0.3} \tag{2.66}$$

In the above equations, V_b is expressed in kV while the electrode separation d is given in millimeters. In the MHz range, however, the breakdown voltage V_b has been shown to depart from the above expressions and follow

$$(V_b)_{ac} = 31d^{0.7} \tag{2.67}$$

where d is the electrode separation for gaps ranging between 1 and 3.5mm.

Chapter 3 Experimental System

As stated earlier, the goal of this thesis was to establish that high field RFQ confinement of ions is feasible and to determine the dynamics of ion collections so confined, with the purpose of setting the principles by which high-field RFQ ion confinement devices could be engineered. To do so, TOF analysis of ions ejected from a linear high-field RFQ trap was chosen to probe the extracted ensembles.

The experimental system designed for this study is shown as a schematic in figure 3.1.

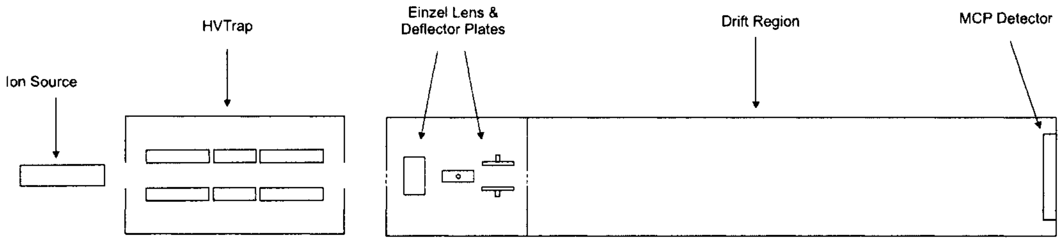

Figure 3.1 Schematic of the experimental apparatus for determining the phase space dynamics of ions in high-field RFQ confinement.

This diagram shows the principle components to be an ion source, the trap and its associated electrical circuits and electronics, an extraction system and its associated electronics, and the TOF detection and data acquisition system.

3.1 Ion Source

Typically, ion sources used in RFQ design or RFQ optimization are chosen to be representative of the ions that will be used in actual experimental research. To provide accurate tests of the confinement the source should produce pure ions of one species, in a steady and reproducible quantity. The ions also should not be sensitive to contaminants in the vacuum system which will make their numbers severely dependent on the vacuum conditions.

Such an ion source is the surface ionization type for alkali metals, which is easily produced by having zeolite vapor pass over heated platinum filaments. The ideal alkali ion for the present study is one which has a mass of roughly 100 amu placing it in the mid-mass region of the ions that would normally be studied in systems that would benefit from high-field RFQ confinement. Such a source was built for this study, based on designs by Ghalambor-Dezfuli [Gha96] and Kim [Kim97]. The design is shown in figure 3.2.

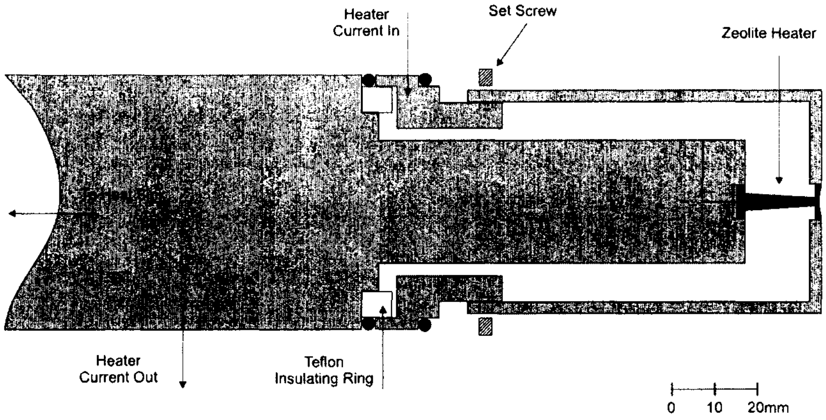

Figure 3.2 **Surface ionization source assembly diagram. Both the zeolite powder and platinum filaments are packed inside the zeolite heater located at the front of the source.**

Unlike the earlier sources used by Ghalambor-Dezfuli and Kim, which were designed to produce ion beams, the one used for this work was placed 5mm from the RFQ's entrance allowing sufficient ions to drift into the HVTrap without prior focusing or beam collimation. As well as avoiding the complicated apparatus associated with collecting and transferring an ion beam into the trap, this considerably simplified the source's design and assembly. However, it also resulted in low efficiency of transfer of the available ions into the trap, requiring the source to operate at much higher production rates than were necessary in the previous works.

The basic mechanism of the operation of surface ionization sources is to bring target atoms, typically from alkali metals, in contact with high work function materials such as tungsten or platinum. Alkali atoms such as Cs, Rb, K, Na and Li have low ionization potentials and are thereby relatively easier to ionize. However, factors such as surface temperature T and the ionizing surface's work function ϕ also have a strong impact on a sample's degree of ionization α. These factors along with the incident atom's ionization potential E^i are related to α as

$$\alpha = Ae^{\left[\frac{z_i(\phi - E^i)}{k_B T}\right]} \tag{3.1}$$

where $A = g_i / g_a$ is the statistical weight ratio of the ionic to the atomic state of the target atoms leaving the ionization surface ($g_i = 1$ and $g_a = 2$ for alkali metals) and z_i is the charge state of the resulting ions [Kin24]. Ultimately, Cesium was determined to be the ideal candidate for the present study in light of its low ionization energy ($E^i = 3.89eV$) and relatively high mass-to-charge ratio (Cs^+; m/z = 133) which makes it fairly easy to identify in TOF mass spectra (figure 3.3). Moreover, cesium ions do not change their charge state very easily with residual molecules or impurities found in the background gas of the trapping system providing the user with very stable particles with which to work.

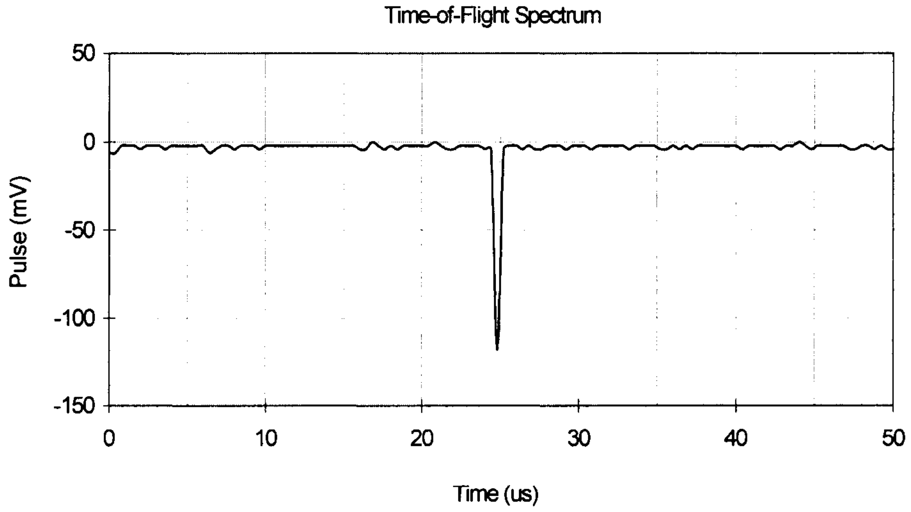

Figure 3.3 **Typical mass spectrum of the Cs zeolite ion source. The mass peaks were calibrate to m/z = 133 corresponding to $_{55}Cs^{133}$.**

The requisite Cs atoms were created by vaporizing a cesium zeolite† sample packed inside a metallic heater made from Inconel 601HF, a steel alloy with high electrical resistivity. Platinum wire (0.127mm diameter, 99.99% purity) was then placed in front of the zeolite sample to ionize the target atoms. Typically, 100W of input power was needed to produce ion currents sufficient for the present studies. Unfortunately, at these power levels the zeolite sample needed to be replaced every 8 to 10 hours to maintain consistent beam currents.

One of the difficulties with these sources was that of reproducibility of operating conditions from one source to the next. This was because of the extreme sensitivity of the temperature of the source to the thickness of the container wall, which had to be thin enough to provide the electrical resistivity needed to generate the heat with a reasonable electrical current, yet thick enough to withstand the erosion of material due to the high temperatures needed. Considerable experimentation therefore had to be carried out on each new source to establish the operating conditions that were appropriate to produce the ions needed for a particular test of the confinement.

3.2 Design of the High Voltage Trap

The basic geometry of the high field RFQ linear trap (dubbed HVTrap) for this work followed that of Fong [Fon01] for his pioneering work on the phase space densities of ion clouds in a linear RFQ trap. The chosen geometry is shown in figure 3.4.

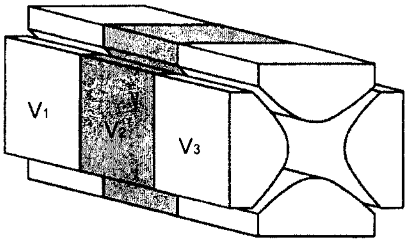

Figure 3.4 The basic geometry of HVTrap

---

† From Greek, meaning "boiling stone".

The differences of this design from that of Fong are that it is smaller, has electrodes that are hyperbolic rather that cylindrical and that it is designed for high voltage operation. The design parameters chosen were an r_0 of 3.125 mm, with an electrode geometry that extended to a gap of 1 mm between adjacent electrodes, with segments that were 10 mm long for the central electrodes and 15 mm long for the end electrodes. The separation between segments is 1 mm. With this geometry, an RF of 7.5 MHz at an amplitude of 4000V between adjacent electrodes gives a q of about 0.27 for cesium ions.

To avoid electrical breakdown all short gaps were free of insulating material with insulators mounted far from the high field regions. In addition, all insulators were of alumina ceramic whereas all electrodes and mounting supports were made out of 304 stainless steel making them very well suited for vacuum environments.

The 12 separate hyperbolically shaped electrodes of the HVTrap are mounted on ceramic insulators to stainless steel backbones (see figure A.1 of appendix A for complete assembly diagram). Each electrode/backbone assembly is then mounted to an outer stainless steel cylindrical support and their positions adjusted to have the same 1mm separation between neighboring assemblies (figure 3.5).

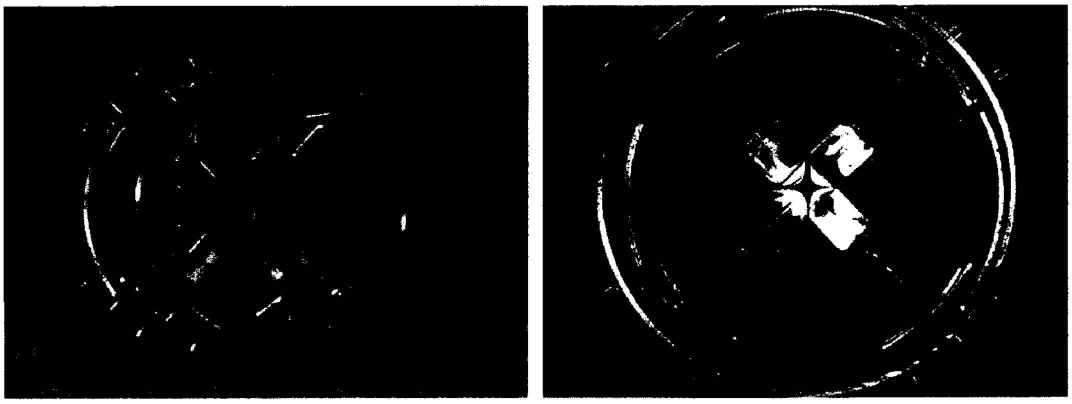

Figure 3.5 The HVTrap (the RF and DC connections are not in place).

The RF is fed to the electrode backbones via a braided cable leading from the external resonant circuit (see figure 3.6). From the backbones it is fed to the individual electrodes via a 1 nF capacitor, capable of withstanding 3 kV. The DC is fed directly to the individual electrodes via cables running through the interior of the braided cable.

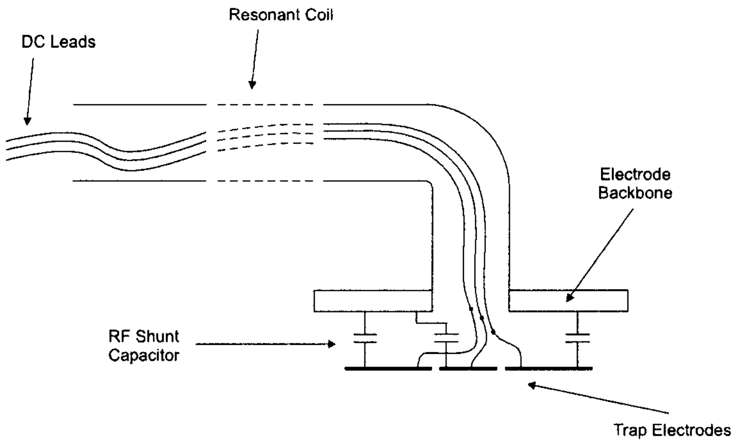

Figure 3.6 Voltage delivery scheme using hollow resonant coils to deliver the RF signal to the quadrupole electrodes. Threaded DC leads are used to deliver the DC voltage to each electrode.

To shield the RF and DC connections to the electrodes from the RF fields between adjacent assemblies, the backbones were equipped with stainless steel shields that covered all but the hyperbolic surface of the electrodes (figure 3.7).

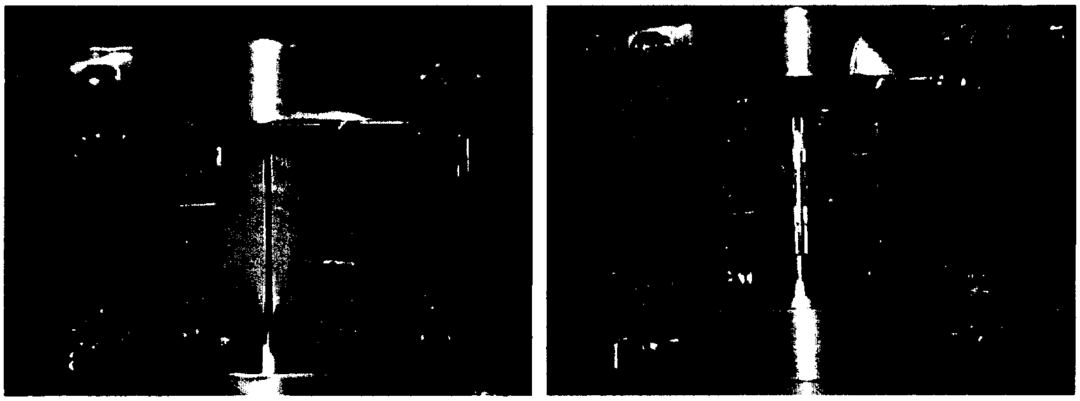

Figure 3.7 a) Shielded backbone assemblies; b) Shields removed exposing shunt capacitors and hyperbolic electrodes.

3.3 Electrical Systems

Linear quadrupole configurations, like the one used for the HVTrap, are only capable of providing radial confinement using axiperiodic quadrupole fields, with no possible trapping along the axial direction. This must be done by providing an axial trapping field, which can be accomplished by segmenting the rod structure and applying appropriate DC potentials to the individual electrodes creating a potential well along the axis capable of collecting and trapping incoming particles (see figure 3.8). These rod segments also provide a perfect way of extracting the confined ions from the trap by pulsing the end electrodes to higher and lower DC potentials creating well-defined beam pulses for detailed analysis by the TOF apparatus.

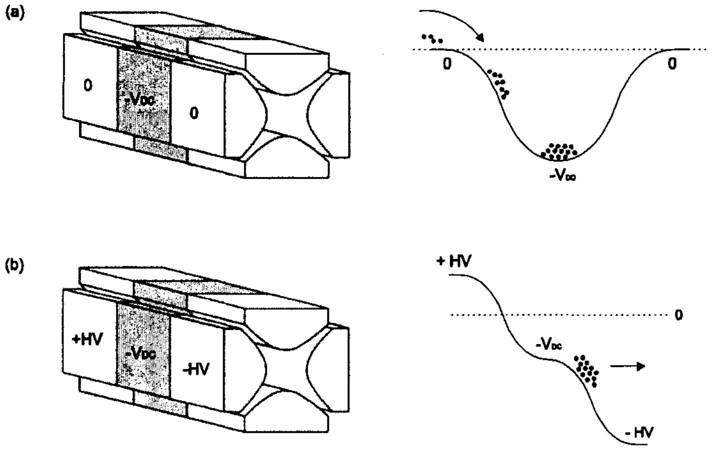

Figure 3.8 A DC voltage scheme for segmented quadrupole rod structures capable of a) trapping then b) pulse ejecting charge particles creating well defined ion bunches.

In order to achieve the high RF potentials across the trap electrodes at reasonable power levels, some form of resonating circuit has to be provided. For the frequencies required for the present work and the load levels presented, the only feasible resonant circuit is a lumped LC split series, as shown in figure 3.9. (For a ferrite cored transformer the frequencies and power levels are too high and for a 1/4-wave resonator the frequencies and load levels are too low.)

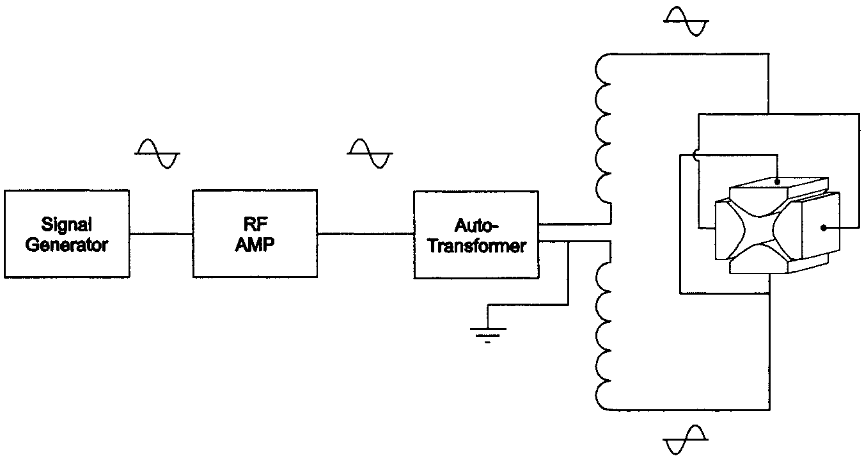

Figure 3.9 Circuit diagram of RF coupling to quadrupole structure.

The primary RF signal used to create the axiperiodic confinement fields within the HVTrap was provided by an SRS DS345 synthesized function generator. This was fed to an IFI 3220 1kW wideband power amplifier. The resulting RF current was then fed to two 10-turn air-cored resonating coils using a 16-turn ferrite auto-transformer. The 4 leads that made up the auto-transformer were wound around 2 ferrite cores (Amidon material #43; 60mm OD) from Amidon Assosiates Inc. These cores, characterized by high volume resistivities and high *Q* factors in the 500 kHz to 100 MHz frequency range, had a rated permeability factor of 850 which made them particularly useful as transformers. While many different coupling transformer configurations were tested, the configuration used for this work was found to have superior impedance matching between the IFI amplifier and the resonating coils, allowing better power delivery through the components.

The air-cored resonating coils, made from standard ¼" copper tubing, were designed to minimize the power losses in the resonating circuit. To reduce the near-field radiation losses from the fringing magnetic fields in nearby conducting materials, the coils were arranged in a toroidal fashion and held in place using a simple acrylic support structure (figure 3.10). In this arrangement, the auto-transformer/resonating coil system displayed a *Q* of 120 which, in the past, had been shown to be sufficient to produce RF potentials of the order of 5kV amplitude at each side of the resonating circuit [Gia02]. To correct for slight imbalances in output voltages from either coil at a given frequency, variable high-voltage vacuum capacitors were placed in parallel at the output of each coil and subsequently adjusted at each operating frequency. This allowed the output voltages from the resonant coils to be balanced within 1% of each other.

Figure 3.10 Resonating coils made from ¼" copper pipe and arranged in a toroidal form.

In this design, the feeding of the DC voltages to the electrodes by threading it through the conductor of the RF resonator is a novel method for superimposing the DC onto the RF of the electrodes. In all previous systems, the superposition was achieved by blocking inductors and shunting capacitors that all had to withstand the full RF potential. However, at the high RF potentials used in the present work this was impossible. Consequently, the leads providing the DC potentials were threaded though the RF resonating conductor so that they could pick up the RF potential at the same time it was picked up by the outer surface of the resonating conductor. Thus, upon arriving at the electrodes it already had the RF potential superimposed on the DC. All that is necessary is for the main RF current to be provided by a shunt capacitor that only has to feed the inter-electrode capacitance of the trap, and withstand any DC voltages between the electrode and the end of the resonating lead. (Preliminary tests of this concept in which an oscilloscope was placed inside a Faraday cage mounted on the end of an LC resonator and connected between the inside of the cage and a lead running up into the cage through the inside of the hollow conductor of the resonating inductor, showed no detectable RF on the lead, proving that, indeed, it had the full RF potential of the cage on it as well.)

To help the Cs^+ ions enter the trap and confine them along the RFQ's axial direction, the back-end electrodes and front-end electrodes were each biased to -6 V_{DC} and +8 V_{DC} respectively. The center electrodes, on the other hand, were biased using a negative 1kV Matsusada variable DC power supply capable of adjusting the trap's axial well depth allowing more (or less) ions to enter the RFQ. In order to extract the confined ions from the trap and send them to the TOF system to the detector, the trap's end electrodes were coupled to high voltage Behlke transistor switches (0.6μs risetime, 10ms falltime) that pulsed the trap's back-end electrodes up and the front-end electrodes down, thereby creating very sharp voltage gradients to push the confined ions out of the RFQ. The extraction voltages used to create these sharp voltage gradients were supplied by two dual polarity variable 3kV Del power supplies and triggered using a second SRS DS345 synthesized function generator. A diagram of the extraction circuit is shown in figure 3.11. While the duty cycle of the extraction pulses was set by the second SRS function generator, the timing of the extraction system was controlled by the primary SRS function generator used to create the AC trapping fields for the RFQ. This allowed one to control precisely when along the RF cycle to extract the ion packet from the trap.

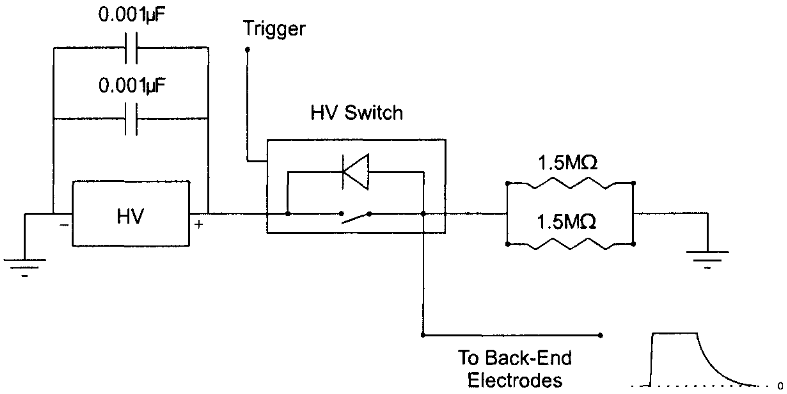

Figure 3.11 Example of the high voltage switching circuit used to pulse the back-end trap electrodes to higher DC potentials. The front-end electrodes used a similar arrangement to pulse the electrodes to lower DC potentials creating sharp extraction gradients to eject ions from the HVTrap.

Because of the relatively high DC voltages required for the fast extraction, the DC leads to the electrodes were high voltage Kapton insulated wires.

In order to monitor the AC voltages across the trap electrodes, the vacuum feedthroughs were threaded through concentric stainless steel pick-off electrodes placed on the vacuum side of the feedthrough connector. Connecting these electrodes, via stiff stainless steel wires feeding through the vacuum port, to 2000pF mica-dipped capacitors located just outside the vacuum chamber, created capacitive dividers that allowed the RF voltages on the electrodes to be monitored without loading the system by any other detector circuit. The RF signals from these capacitor dividers were then sent to an oscilloscope via BNC connectors and selected lengths of standard 50Ω coaxial cable (figure 3.12). The ratio of these capacitive dividers was then calibrated using a known signal attached to the RF connectors.

Figure 3.12 High voltage feedthrough assembly used to deliver the AC/DC potentials to the HVTrap and monitor the RF signal. Variable vacuum capacitors on either side of the assembly provide a simple way of tuning the resonant frequency and balancing the RF voltages.

3.4 Time-of-Flight/Detection System

The Time-of-Flight (TOF) system, starting at about 10 mm away from the HVTrap exit, consisted mainly of a 1m stainless steel drift tube (70mm OD, 66mm ID) coupled to a negatively biased dual polarity high voltage supply. Typically operated at $-1800V_{DC}$, the drift tube voltage could be manually adjusted down to -2500V_{DC} enabling users to vary the kinetic energy of extracted ion packets. To focus the extracted ions onto the detector and to compensate for misalignment of the HVTrap and the TOF system, an einzel lens and two sets of parallel deflection plates (orthogonal to one another) were placed at the start of the drift region. These steered and focused the extracted Cs ions onto the detection system. Schematics for the einzel lens and deflector plates can be found in figure A.3 of appendix A. The DC supplies used to power the einzel lens and the deflector plates were grounded with respect to the flight tube and were able to supply 0-1.2kV_{DC} on top of the drift tube bias. Voltage divider circuits were used to split the 0-1.2kV_{DC} between the deflector plates so that the middle plane between each set of deflector plates had the same voltage as the drift tube, ensuring that ions passing exactly on axis did not experience any acceleration in the axial direction as they traveled towards the detection system.

The high time-resolution detection system used to examine the extracted ion packets from the HVTrap was the same one used by Fong [Fon01] in his study of the phase space densities of trapped ion clouds, and is shown in figure 3.13. Composed of two chevron-stacked Galileo microchannel plates (MCP), the detector is characterized with fast rise-times for accurate event timing and high amplification for detecting small numbers of incoming ions. The MCPs are mounted on a custom-made "slim profile" assembly designed to eliminate signal delays and reduce noise from surrounding sources. For a detailed description of the MCP assembly see [Fon01]. For optimal signal detection, the MCP assembly was biased so as to achieve a 1kV_{DC} drop across each plate. The resulting electron shower produced by impinging ions are then collected by a stainless steel anode and generates a distinctive signal of the original incoming ion packet. The resulting signal is then collected and digitized by a Fluke 199 digital oscilloscope for later analysis.

Since the ion signals produced by the MCP detector were strong enough to be seen by the Fluke digital scope directly, no amplification of the MCP pulse was necessary. To calibrate the resulting MCP ion signals and determine the number of Cs ions contained in each pulse, single-ion counts were performed by setting the digital scope to "single shot" mode and recording incoming signal bursts. For this to work, however, the ion source's input power needed to be dialed down slowly and operated at the very limit of the zeolite's ionization temperature ensuring that only a few Cs ions were created and trapped by the HVTrap. A representative signal of a single ion is shown in figure 3.14. After collecting hundreds of single-ion counts and averaging out the area under each principal peak, areas for single ion pulses were measured to be on average $(3.41 \pm 0.15) \times 10^{-11}$ *V-s*.

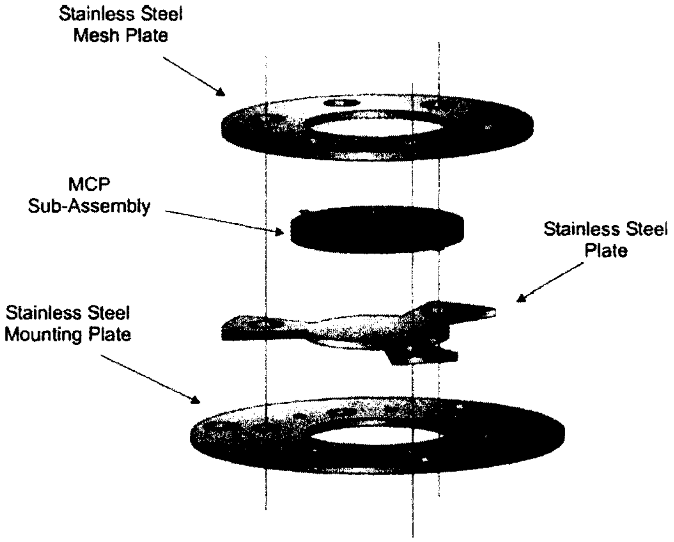

Figure 3.13 Assembly diagram of MCP detector used to record arrival times of ion packets.

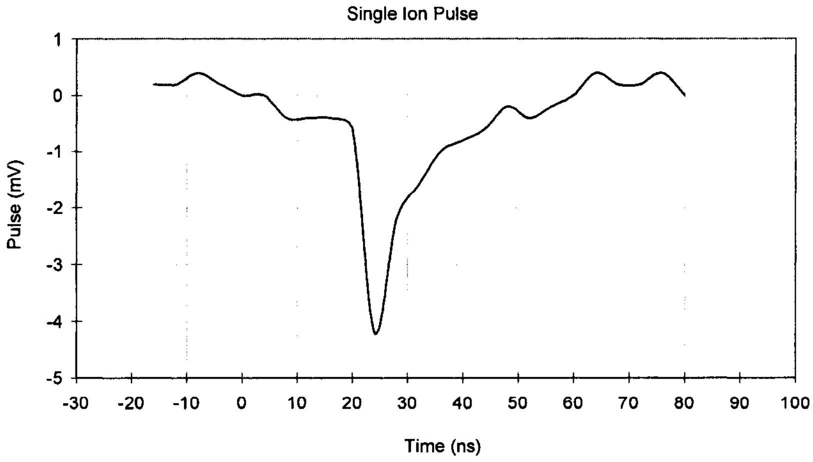

Figure 3.14 Typical signal of a single Cs ion striking the MCP detector.

To eliminate background noise from recorded TOF signals and smooth out overall pulses, the Fluke digital scope was operated in "signal averaging" mode throughout the entire study. Naturally, using more ion pulses to average out the final signal would result in less noise and smoother curves but given the relatively short life times of the zeolite ion source samples and the need to keep ion beam currents relatively stable throughout separate runs, each signal could not be averaged for extended periods of time. This resulted in small but discernible RF noise on recorded ion signals from the MCP detector.

3.5 Vacuum System

The vacuum system used to investigate the HVTrap's performance (figure 3.15) implemented a differential pumping scheme capable of operating two separate pressure regimes simultaneously. While the microchannel plate detector needed to be operated at a few μTorr to reduce signal noise and prevent electrical damage, the HVTrap would have to be tested at various buffer gas pressures to investigate the effects of collisional cooling on the confined Cs ions. To avoid overloading the vacuum system, two Varian V250 turbo pumps (250L/s) backed by Alcatel 2015 mechanical pumps were installed at either end of the system while the Time-of-Flight tube was completely sealed at the front end of the drift region except, of course, for the 6mm opening used to send ion bunches from the HVTrap to the MCP detector (see einzel lens assembly diagram in appendix A).

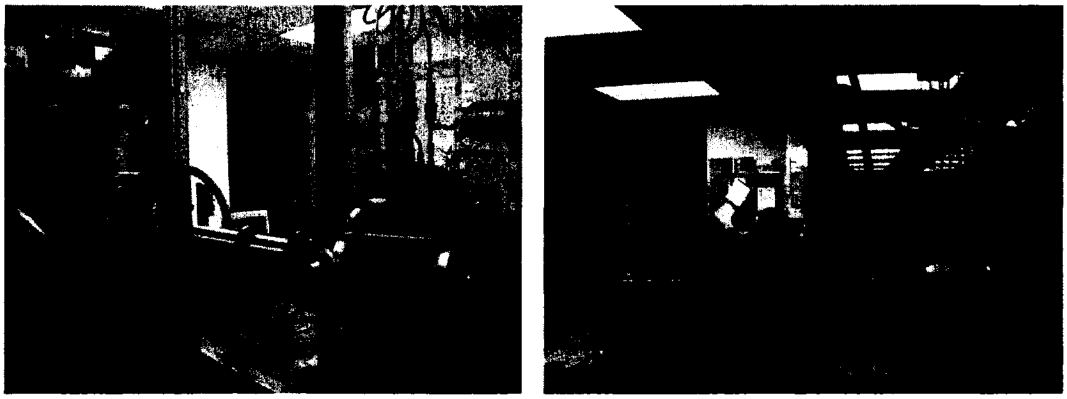

Figure 3.15 Side views of the complete experimental setup.

The first turbo pump, located just underneath the main chamber used to house the HVTrap, typically reached base pressures of 3μTorr whereas the second turbo pump, place just above the MCP assembly, reached base pressures of 2μTorr. While this was more than adequate to operate the MCP detector without any problems, low vacuum pressures in the drift region were essential to eliminate any scattering of the ions by any residual background gas in their path to the MCP detector.

To introduce small amounts of buffer gas into the trapping region, a Nupro SS-4BMG needle valve was used to adjust the system's helium gas intake. Pressure levels were monitored using a series of thermo-couple gauges installed throughout the entire setup and two Varian 571 BA ionization gauges placed at either end of the experimental system.

Chapter 4 Computer Modeling of the TOF Signals

An essential part of using TOF spectrometry to probe the phase space of an ion collection in a trap is mathematical modeling of the ion collection in the trap and its behaviour on its flight to the TOF detector. It is only in this way that information can be extracted from the TOF signals about the actual phase space volume of the collection while it is in the trap. The procedure is iterative in that a certain model of the cloud is adopted and this model is tracked to the detector to simulate a signal. This signal is then compared to the observed signal and the model of the collection in the trap is altered until simulated signal matches the observed signal, to within the accuracy of the observation.

The model of the trap collection adopted in the present work is that of an ensemble of ions in thermodynamic equilibrium while under confinement that causes the ions to execute simple harmonic motion, all at the same frequency but at random phases and amplitudes, where the amplitudes have a distribution that is Gaussian (2.37). The pioneering work of Lunney [Lun92], followed by Ghalambor-Dezfuli [Gha96], Kim [Kim97], and Fong [Fon01] have all confirmed that this is a good model of collections of ions under RFQ confinement in buffer gas, at least at relatively low RFQ fields, and there is no reason to believe that it would be a good model for high fields.

In a linear RFQ trap there are two kinds of confinement; the axial confinement due to the DC potentials applied to the end electrodes and the transverse confinement due to the RFQ field. Thermal equilibrium of the ion collection, however, assumes that the temperature in the axial degree of freedom is the same as in the radial and so the temperature in only one of these dimensions needs to be determined. In the works of Lunney, Ghalambori and Fong only the axial temperatures were probed, although rough estimates of the transverse temperatures indicated that they could not be significantly different. Alternately, the work of Kim measured only the transverse temperature, but again, limits that could be placed on the axial temperatures indicated that they could not be significantly different from the transverse. Indeed, for the same degree of confinement, the work of Kim showed temperatures that were similar to those of Lunney and the others.

While, ideally, both temperatures should be measured so as to support the model of the ion collection being in thermal equilibrium, this is extremely difficult to do simultaneously. This is because the measurement of the transverse temperature requires careful probing of the beam cross-section along with accurate simulations of the ion trajectories off-axis. Accurate simulation of the off-axis trajectories is extremely time consuming since they have to be carried out for all possible phases of the RFQ field for each of the ions in the randomized collection and averaged so as to simulate the observed beam cross-section. For a full account of the problems involved, see Kim [Kim97]. The present work therefore follows that of Lunney, Ghalambori and Fong in using only TOF to determine the axial temperature of the ions.

The axial confinement can be described as a potential well, the shape of which is shown in figure 4.1.

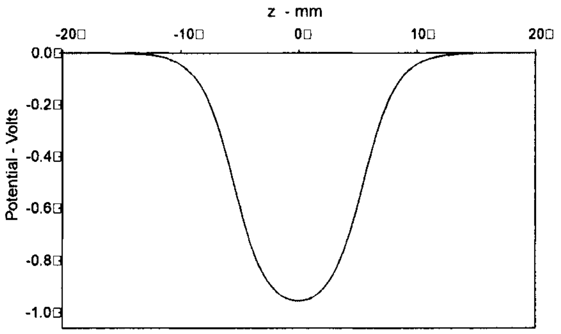

Figure 4.1 The potential on the axis of the trap as a function of distance from the trap center, for one volt on the center electrodes.

In general, this potential function can be expressed as a polynomial

$$V(0,z) = V_{DC}\left(a + bz + cz^2 + \ \ldots.\right) \tag{4.1}$$

By setting the potential at the center of the trap to zero, and the z-coordinate so that it is zero at zero slope of the potential, (4.1) becomes

$$V(0,z) = V_{DC}\left(cz^2 + \ \ldots.\right) \tag{4.2}$$

For small excursions from the trap center, as is expected in high-field confinement, the higher order terms of the polynomial become insignificant and the potential well induces simple harmonic motion of angular frequency

$$\omega_z = \sqrt{2cV_{DC}\frac{e}{m}} \tag{4.3}$$

for singly charged ions of electrical charge e.

This value of ω_z enables a modeling of the trap collection in axial phase space for a particular temperature T according to the equations (2.40). For the present work this model was a statistical ensemble of 1000 particles distributed throughout the action diagram according to (2.37). By taking the spatial and momentum units as their standard deviations, their values in physical units could be simply scaled to all temperatures and angular oscillation frequencies. This basic ensemble, created using an MS Excel spreadsheet, is shown in figure 4.2. In generating a model of the ion cloud for a particular set of operating conditions of the trap and for a specific temperature the values of position and momentum for each of the 1000 particles were then multiplied by the values for the standard deviation parameters for that situation. These action coordinates were then exported to the computer program for simulating the flight of the ions during extraction to the TOF system.

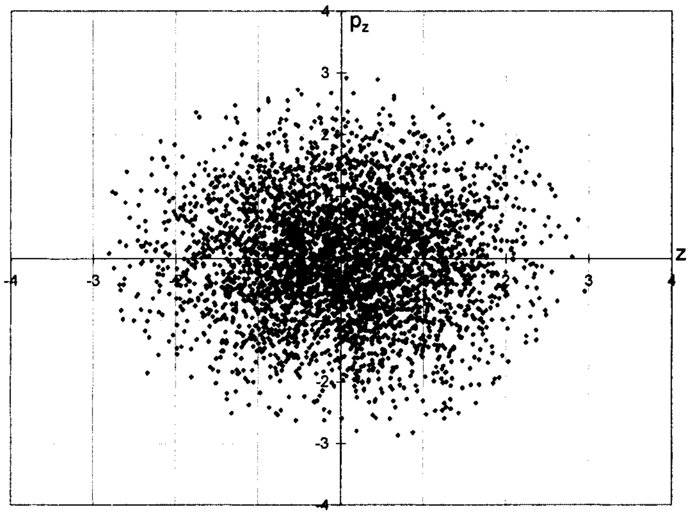

Figure 4.2 Random array of position and momentum coordinates used to simulate a thermalized Cs ion ensemble. This array is generated in units of standard deviation σ_z and σ_{p_z}.

The computer program used for simulating the ion extraction was SIMION 7.0, a finite-difference software package based on successive over-relaxation[†]. The model of the electrode configuration used in this program is shown in figure 4.3.

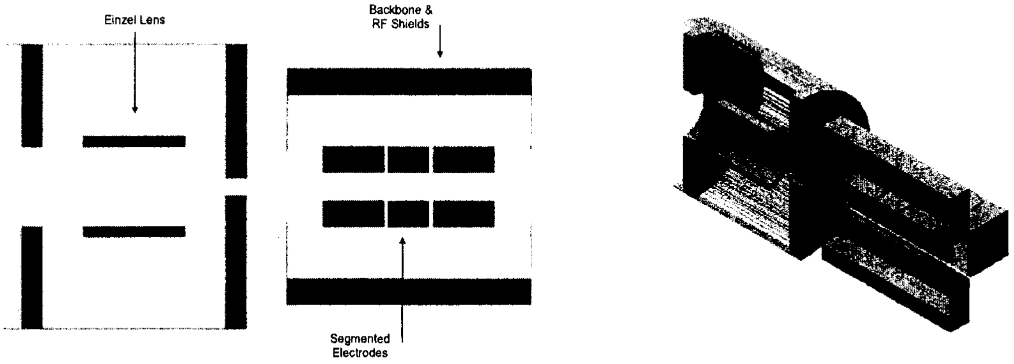

Figure 4.3 Cross-sectional views of the SIMION potential array used to model the trapping and extraction voltages for the HVTrap. (Here the ions travel from right to left.)

For this geometry, SIMION calculated the value of c to be 0.0143mm^{-2}. Using this value, together with the potential applied to the central electrodes of the trap, the angular frequency of the axial oscillations could be calculated and the extraction of the ion collection could be simulated.

Once the ion cloud had exited the extraction region, and thereby entered the field-free TOF region, their trajectories to the TOF detector were taken to be simply straight lines. Field imperfections resulting from stray external fields entering the drift region were assumed to be unimportant as were ion-background gas collisions capable of perturbing an ion's motion in the TOF system. At $2.5\times10^{-6}\,Torr$, the mean free path of a Cs^+ ion in a 1-m drift tube was evaluated to be roughly 25m [Hal88], suggesting that collisions between an ion ensemble and background gas molecules are in indeed negligible.

As each ion reaches the MCP detector plane, its arrival time is binned appropriately, creating a time-of-flight histogram for each extracted ensemble that simulates the

---

[†] Non-electrode points in a three dimensional array are successively approximated by averaging the potential values of neighboring points [Dah95].

experimental ion signal recorded by the MCP detector. Figure 4.4 shows the simulated signal for three different temperatures of the model of the trap collection compared with the actual signal from the MCP detector.

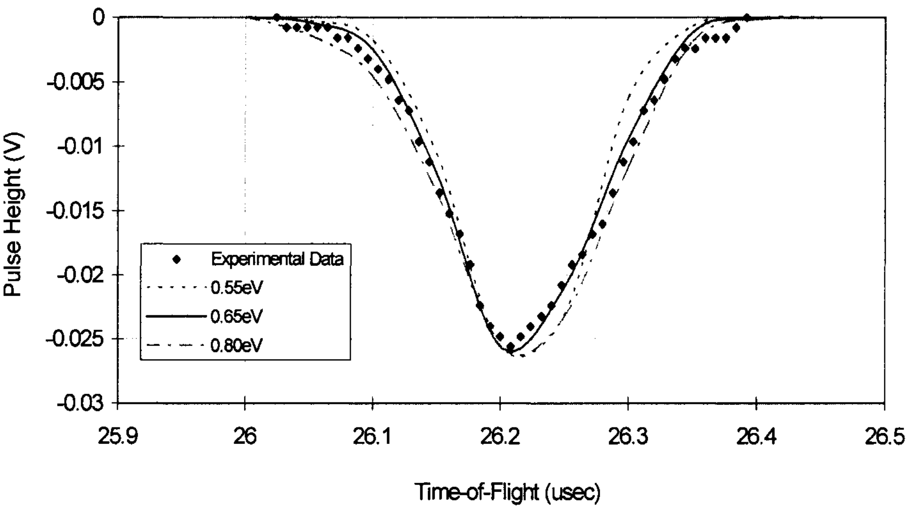

Figure 4.4 Simulated temperature curves and experimental data taken at 2650 V_{RF} and -70 V_{DC} axial well depth. The extraction voltages were set at ± 600V.

The only adjustable parameters in this fit are the amplitude of the observed signal and a very minor shift (about 0.03 μs) in the horizontal position of the peak of the observed signal, no doubt due to uncertainties in the actual rise-time of the extraction electric field.

While the radial confinement was not probed in the present work, it is of importance in determining the profile of the beam at the TOF detector, and hence in determining the proportion of the ion collection that reaches the detector. While the radial confinement is not a true electric potential well, the macromotion of the conferment is simple harmonic and so can be treated as arising from confinement in a potential well. Such a well is referred to as a "pseudepotential well", and is of functional form

$$V(r)_{RF} = \frac{qV_{RF}}{8r_0^2} r^2 \tag{4.4}$$

where q is, again, the Mathieu parameter for RFQ confinement.

However, in a linear trap the DC field of the axial confinement has a radial component that is deconfining. The actual form of the pseudopotential well in axial and transverse coordinates is then

$$V(r,z)=c\left(z^2-\frac{r^2}{2}\right)V_{DC}+\frac{qV_{RF}}{8r_0^2}r^2 \tag{4.5}$$

A trial calculation of the trajectories of a representative collection of ions in such a pseudopotential well, gave the results shown in figure 4.5.

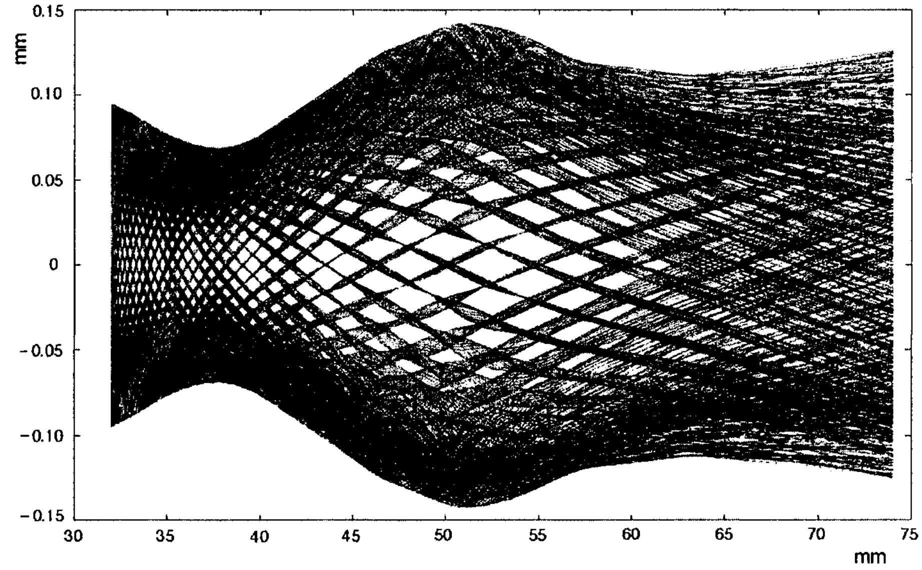

Figure 4.5 Simulated trajectories of ions extracted from the linear trap of this work. when they have a temperature of 0.2 eV at the moment extraction is applied.

This calculation was preliminary to the actual experimental work to ascertain that the TOF transport and detector system would be adequate for the size of beam. The operating parameters of the trap were as extreme as thought to be feasible, i.e., RF of 9 MHz at 4000V amplitude across adjacent electrodes. The various families of curves were for ions equally spaced on the edge of the elliptical action diagram for an oscillation energy of 60 meV. The various curves within each family are for different RF phases at the start of the extraction. The calculation ends in the field free region of the TOF tube. There the divergence of the beam is about 2 mrad, leading to a beam diameter of about 5 mm at the TOF detector.

Although it was expected that a typical temperature of the ions in the high-field trap would be much greater than 60 meV, the beam diameter for higher energies, in the absence of non-linear effects, scales as the square root of the energy. Thus it is expected that, for example, at a temperature of 0.5 eV about 50% of the beam should fall within the active area of the detector.

This was confirmed by subsequent experimental work where the deflector plates were used to scan a beam over the detector. However, to turn such an experimental procedure into an accurate probe of the transverse action diagram would require a much more careful scanning of the beam in the two transverse dimensions. This is because, as demonstrated by Kim, and seen by other workers probing the beams from mass filters, a beam extracted from RFQ confinement is not a circle but more like a four-leaf clover. Simulating the pattern for the extraction of one collection of ions at a given ion temperature therefore requires many more trajectory calculations than those needed for simulating the TOF signal, which in itself was quite time consuming because of the large library of data files and the time required to reproduce each TOF signal.

Chapter 5 Results & Discussion

To determine whether stable operation of high-field RFQ confinement in a buffer gas was feasible and to determine the phase space density of ion collections that can be achieved under various operating conditions and numbers of collected ions a standard set of operating conditions was selected for the operations of the trap.

5.1 Operating Conditions

The default operating parameters for the HVTrap are summarized in table 5.1. One of the parameters that was varied very rarely is the resonant frequency. This was because of the difficulty of tuning the high voltage vacuum capacitors that paralleled the trap electrodes so that, at a chosen resonant frequency, the two sides of the resonating circuit were balanced. The most frequently used method for altering the strength of the RFQ confinement was therefore to simply change the RF amplitude. The method for altering the axial confinement strength was, of course, to simply adjust the DC potential applied to the central trap electrodes.

Operating Parameters	Default Value
Resonant Frequency	7.52 MHz
Trapping Region Base Pressure	$3.0\text{x}10^{-6}$ Torr
TOF Region Base Pressure	$2.5\text{x}10^{-6}$ Torr
Collection Time / Extraction Period	1 second
Extraction Voltages	±600V
TOF Bias Voltage	-1.8kV

Table 5.1 HVTrap's default operating conditions.

Because of variability of the ion source over longer periods, the TOF signals were averaged over 100 extraction pulses, i.e., over a period of 100 seconds. From figure 4.4 it can be seen that this gave adequate smoothness for the TOF signal.

5.2 Axial Well Depth

In order to carefully investigate the effects of the axial well depth on the number of confined ions, the HVTrap's middle electrodes were DC biased in the range from -10V to -150V. While increasing the RF potential across the electrode assemblies provides stronger radial confinement for incoming ion beams, appropriate DC voltages are needed on the individual trap electrodes to confine and bunch these stronger beams. If the axial well depth is too shallow, the RFQ will saturate quickly resulting in very few ions being confined. Figure 5.1 shows that increasing the DC bias on the middle electrodes, thereby deepening the axial well, allowed more ions to be trapped. However, continuing to increase the well depth causes a defocusing of the ion ensemble in the radial direction that counteracts the RF confinement and leads to a loss of ions. A peak is therefore reached when the balance between the axial confinement and the radial confinement is optimized. As can be seen from figure 5.1, this peak rises in well depth as the RF amplitude rises. Also, as expected, the peak corresponds to greater number of ions stored with increased RF amplitude.

A plot of the number of ions stored as a function of RF amplitude, at optimal axial confinement, is shown in figure 5.2 showing the extreme importance of strong RFQ confinement for being able to hold large numbers of ions.

It is interesting to note how the optimal DC bias needed to trap the maximum number of ions at a given RF potential increases with greater RF voltages across the HVTrap's electrodes. Because of the HVTrap's tight configuration, greater RF potentials tend to squeeze the ions radially, forcing them into the trap's axial direction and potentially out the RFQ's ends. To counteract these forces, the axial well depth must be increased as well to pull the ions back into the center of the trapping region. Here space charge effects could be important. Calculations performed by Guan and Marshall [Gua94] have shown that the space charge potentials generated by larger ion ensembles can cancel part of the RFQ's total trapping potential resulting in a shallower pseudopotential well and a radial spreading of the ion ensemble within the trap.

To check whether a confined ensemble's space charge might have affected the optimal DC bias at a given RF potential, the optimum axial well depth for given RF amplitudes was tested using lower input beam currents which resulted in fewer ions in the trap. These ion collections were roughly 10 to 20 times smaller than those of figure 5.1. The results are shown in figure 5.3. From this figure, the optimal DC biases needed to trap these smaller collections are not significantly different from those for the larger ensembles indicating that space charge does not significantly affect the balance between the radial and the axial confinement.

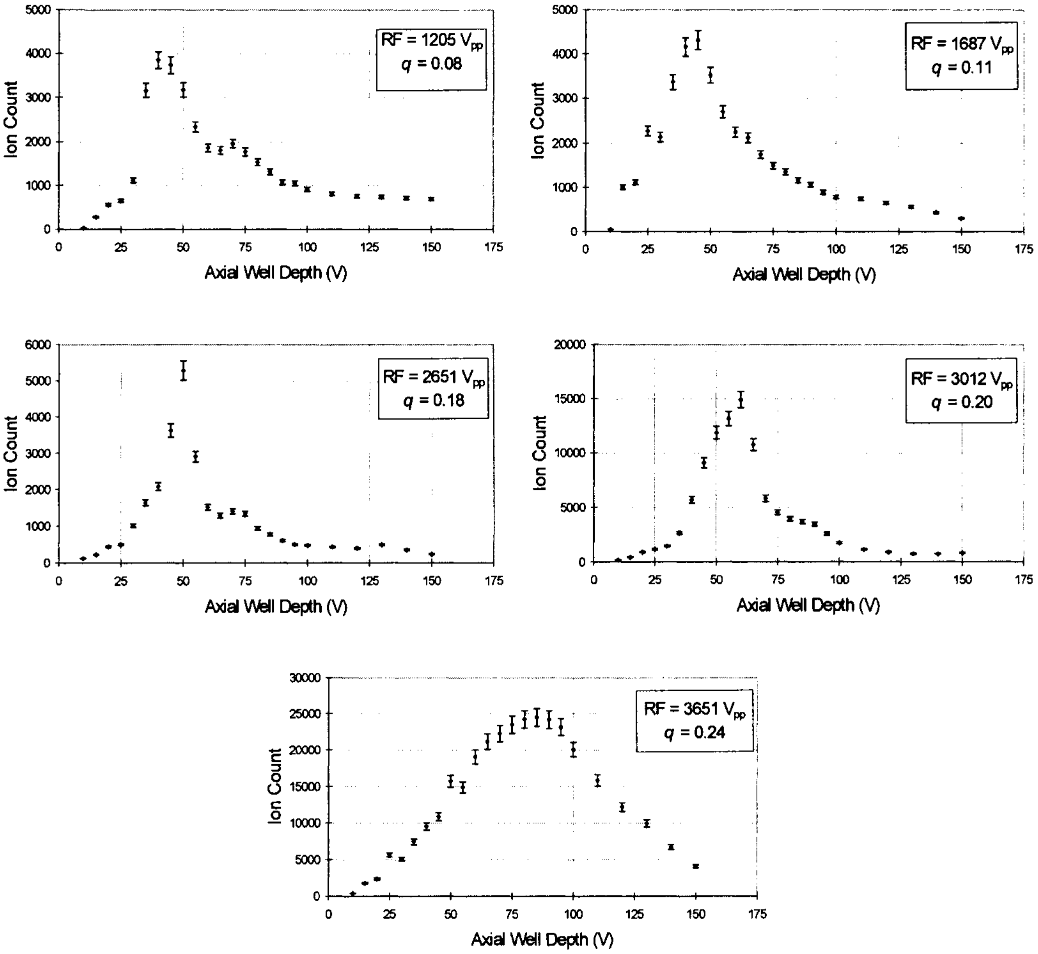

Figure 5.1 The number of detected ions versus the axial well depth at various RF voltages.

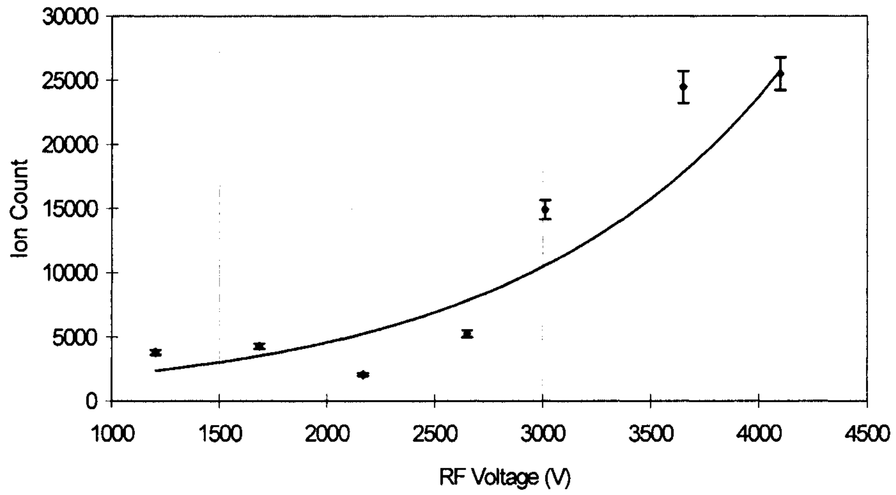

Figure 5.2 The maximum number of detected ions as a function of the HVTrap's applied RF voltages. The trendline was generated using a polynomial fit to the data points.

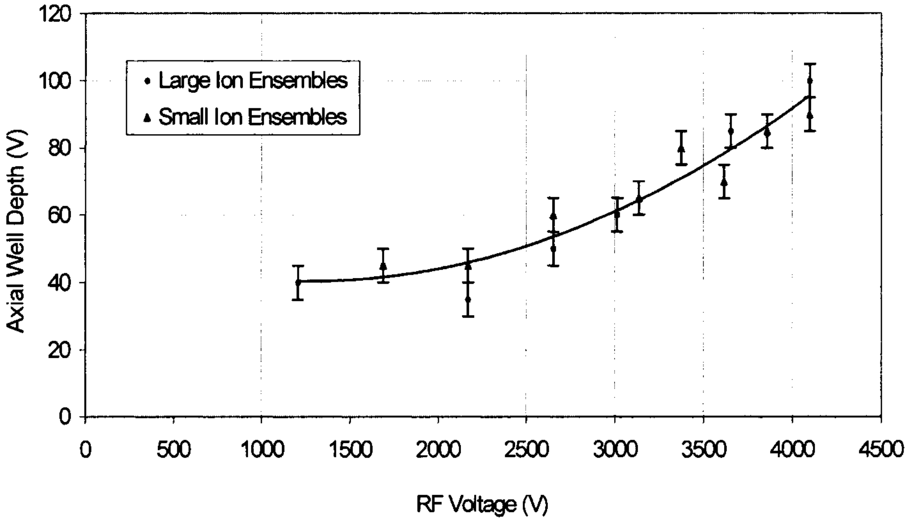

Figure 5.3 Optimal axial well depth needed at various RF voltages to confine the maximum number of Cs^+ ions for two different ion source currents. The trendline was generated using a polynomial fit to the data points.

However, the TOF signals for the heavier loadings do show evidence of space charge effects. These signals are shown in figure 5.4 for various axial trapping voltages at an RF amplitude of 3615 V.

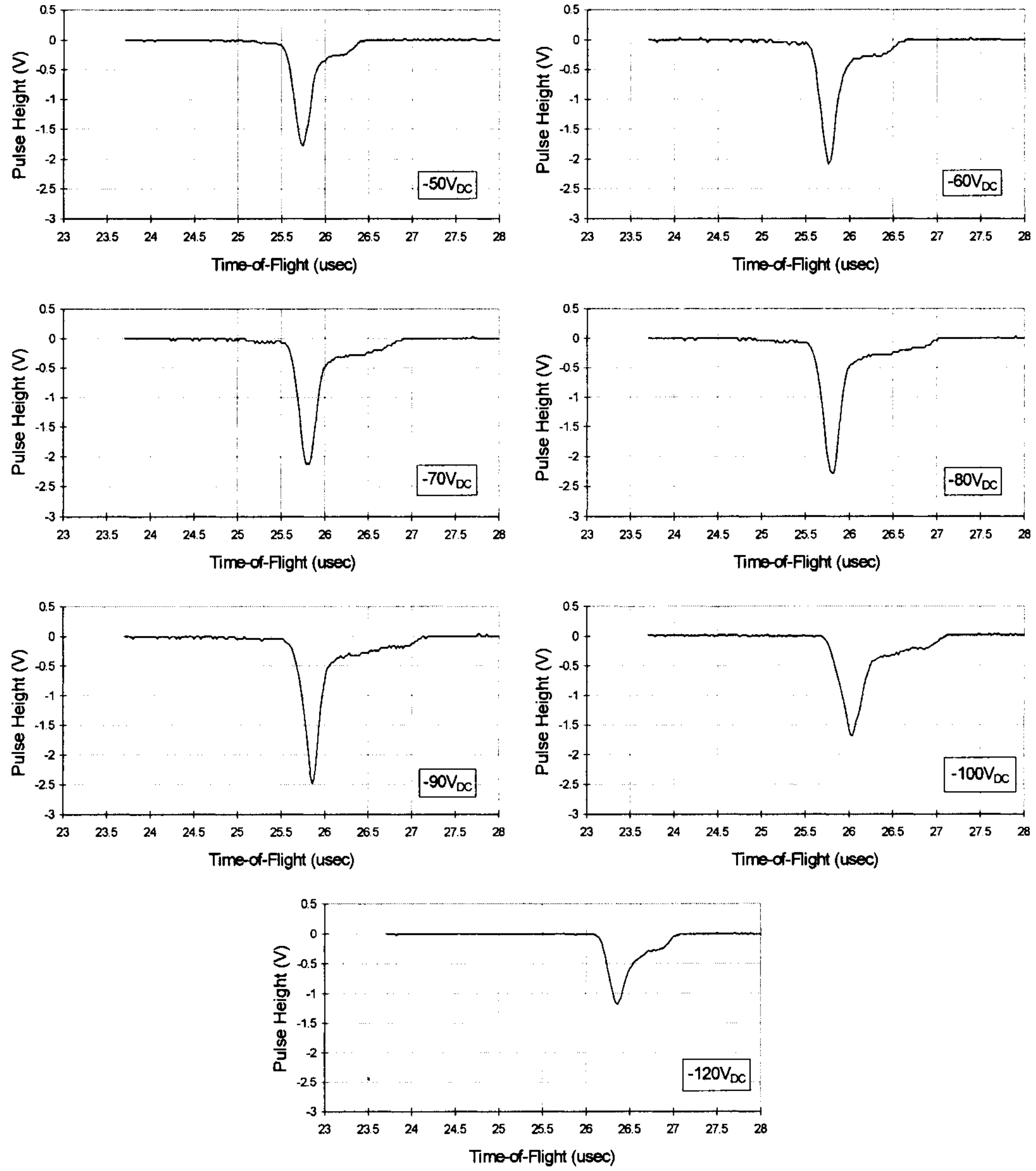

Figure 5.4 TOF signals with various axial trapping potentials for 3615V$_{RF}$.

The significant number of ions exiting the trap after the main peak can be explained by the method of loading of the trap. In order to attract ions into the trap from the source, the entrance end electrodes of the trap were biased downward by 6 volts. On the other hand, to not have them fly through the trap the exit end electrodes were biased up by 8 volts. For the loading method chosen for the present work it was found that this was the only way in which sufficient quantities of ions could be loaded into the trap.

Although this produced a slight asymmetry in the axial confinement, it did not affect the parameter *c* of equation (4.3). However, it did introduce the possibility of ions being "parked" in the set of electrodes at the trap entrance once the trap was filled. To the trap side they faced the space charge repulsion of the ions already in the trap and to the ion source side they faced the uphill potential of 6 volts (figure 5.5).

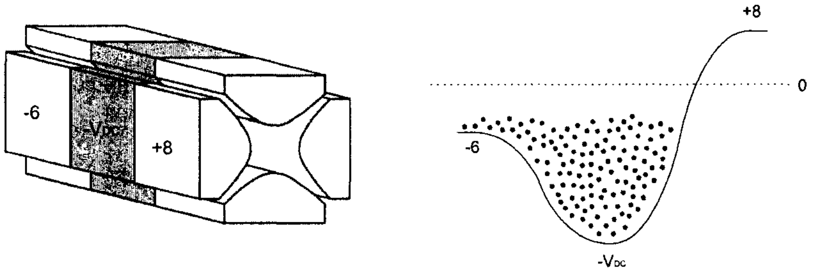

Figure 5.5 The parking of ions in the entrance electrodes of the trap at high trap loading. For clarity, the biasing of the entrance and exit electrodes is exaggerated compared to the trapping well depth.

This parking of ions at the trap entrance was only noticeable when the number of detected ions rose above 15,000. For an expected detector efficiency of the order of 50%, this indicated that the useful limit for number of ions stored is of the order of 30,000.

5.3 Duration of Collection

One of the concerns in measuring the temperature of an ion collection is determining whether or not the collection has reached thermal equilibrium at the moment of extraction. Of course, with continuous filling, as in the present work, the last ions to enter the trap will not be cooled. What is required then is to establish that these are an insignificant fraction of the total collection.

Past reports have indicated that cooling times of the order of a few tens of milliseconds were typically needed to adequately thermalize large collections of ions [Gha96] [Kim97] [Fong01]. These figures, however, are highly dependent on the pressure of the cooling gas. Also, it is not known how these cooling times would be affected by the high RFQ fields applied in the present work. Consequently tests were carried out at a variety of collection periods. A representative cycle of the collection period is shown in figure 5.6.

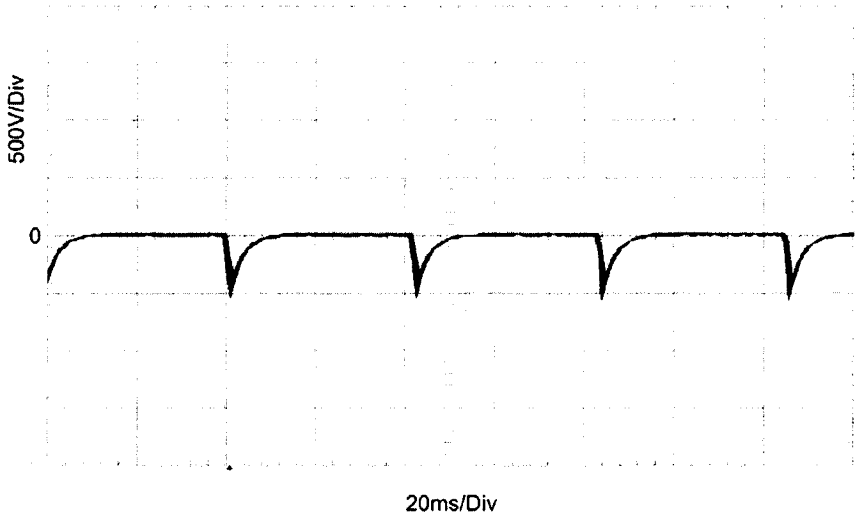

Figure 5.6 A representative collection/extraction period used to collect, cool and extract ion ensembles from HVTrap.

Setting the ion source current to moderate, the number of ions extracted was observed for various collection times and various buffer gas pressures. The results are shown in figure 5.7 and 5.8.

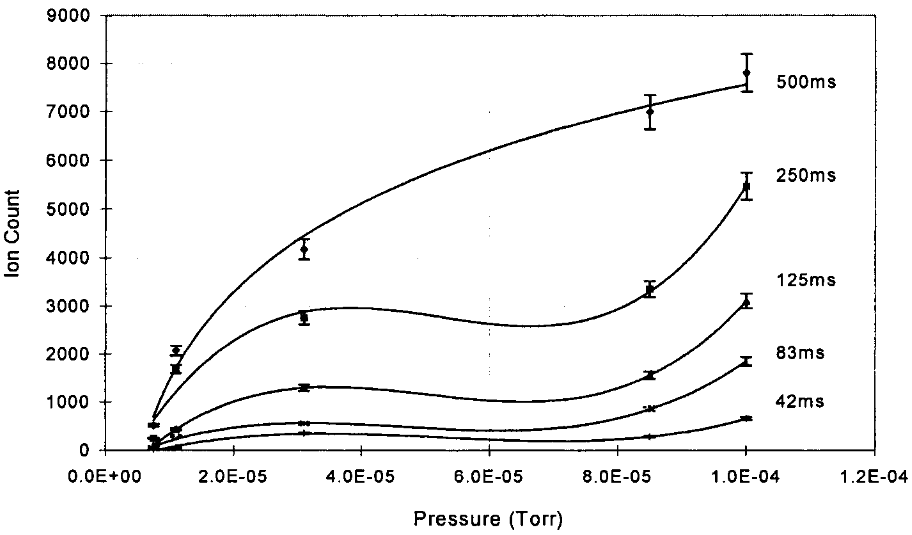

Figure 5.7 The number of detected ions as a function of the helium buffer gas pressure present in the trapping environment. The trendlines for the 42-250ms datasets were generated using a polynomial fit to the data points while the 500ms dataset used a logarithmic fit.

As expected, the introduction of buffer gas significantly raised the collection efficiency of the trap, with indications that the collection and cooling efficiency would be further improved at pressures even higher than the maximum of 10^{-4} Torr that could be accommodated by the present vacuum system.

The dependence of the number of accumulated ions on the collection time is shown in figure 5.8. Except for an anomaly, unexplained, at a gas pressure of 8.5×10^{-4} Torr, the trendlines for the cooling gas pressures of pressures of 10^{-4} Torr and above all show evidence of the ion count plateauing at collection times of 500 ms suggesting a saturation and thermalization of the confined the ion cloud.

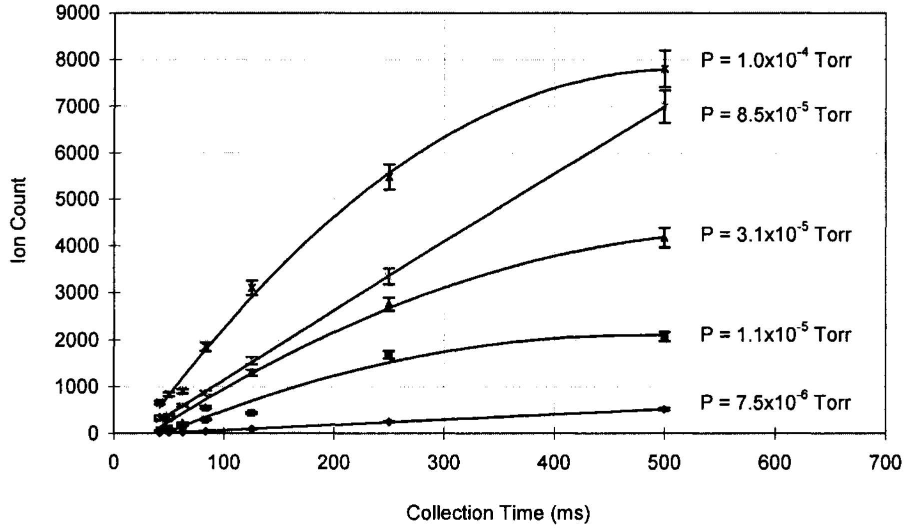

Figure 5.8 Effects of collection time on the number of detected ions at various cooling gas pressures. The trendlines were generated using a polynomial fit to the data points.

5.4 Extraction Voltages

As shown in chapter 2, the TOF signal of a collection on ions extracted from a region where their center of mass is at rest will depend on the electric field that is used for their extraction. For the present studies it is therefore necessary to determine the most favourable extraction field. For this reason tests were carried out as to the TOF and the detection efficiency as functions of the extraction field. While the high voltage switching circuit used to apply the extraction field could switch up to ±3kV, extraction voltages were never taken past ±1kV to prevent possible damage to the Kapton insulted wires leading these potentials through the resonating coils to the trap electrodes. (Higher voltages would have required wires with thicker insulation that would have made them very difficult to thread through the coils.)

Figure 5.9 shows the resulting time-of-flight of ion collections at various extraction voltages. As expected, the larger extraction gradients produced shorter times-of-flight due to the larger accelerations experienced by the ion bunches before entering the TOF system.

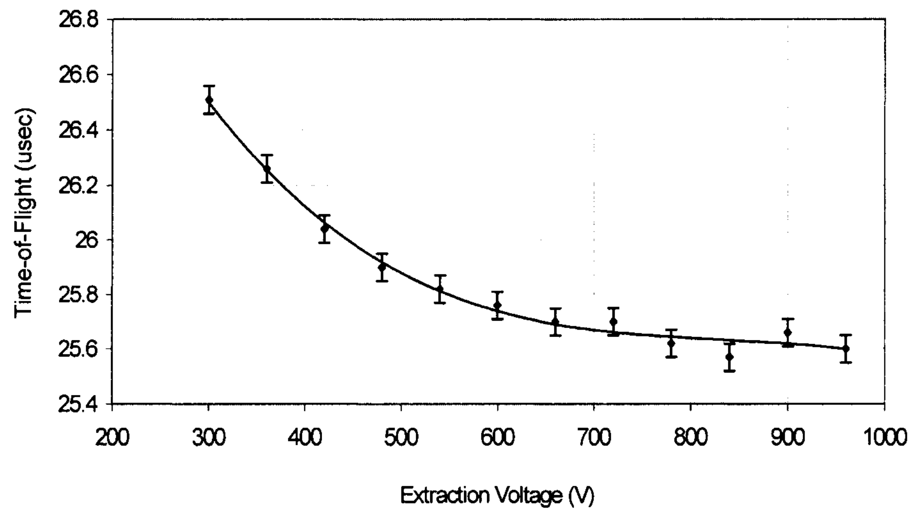

Figure 5.9. Average TOF of ion collections as a function of extraction voltage, applied equally to the entrance and exit end electrodes. The trendline was generated using a polynomial fit to the data points.

Figure 5.10 shows the ion count at the MCP detector as a function of extraction voltage. The variation shown here is due to the optics of the ion beam in its flight to the detector, where higher extraction voltages lead to better focusing of the ions onto the detector and a more efficient collection.

From figure 5.10 it would appear that extraction potentials beyond 1000 volts would be more appropriate for delivering the ions to the detector. However, this was regarded as unsafe for the wires providing the extraction potentials to the electrodes. The operating extraction potential was therefore chosen to be ±600V, where the detection efficiency was a slowly varying function of the voltage. From figure 5.9, this was a voltage at which the TOF was also not a very steep function of the extraction voltage.

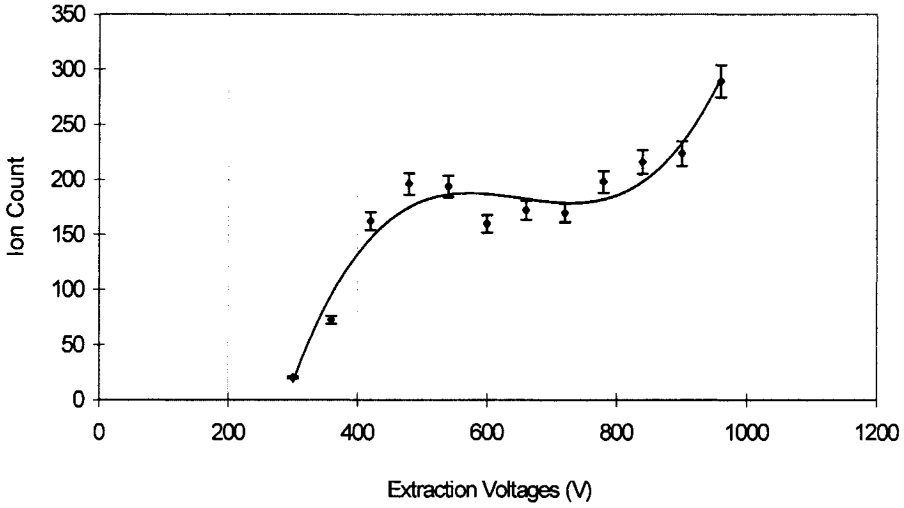

Figure 5.10 **The ion count measured at various extraction voltages. The trendline was generated using a polynomial fit to the data points.**

Although it was not a significant component of the present work, the detection efficiency at this extraction voltage, obtained by sweeping the beam across the detector using the deflection plates, was estimated to be of the order of 50%.

5.5 TOF Pulse Width as a Function of Trap Loading

Preparatory to detailed study of the ion temperatures, the TOF pulse width was observed for various trap loadings, well below the limit at which the parking of ions occurred (figure 5.4). For the standard collection time of 500 ms and extraction voltage of ±600V, the results are shown in figure 5.11. In this figure, the time spread only increases by about 30% for a trap loading that increased by a factor of 7.

This was encouraging in that the primary factor in determining the temperature of the ion collections appeared not to be the space charge of the ions, about which nothing can be done, but rather the influence of the confining electrodes.

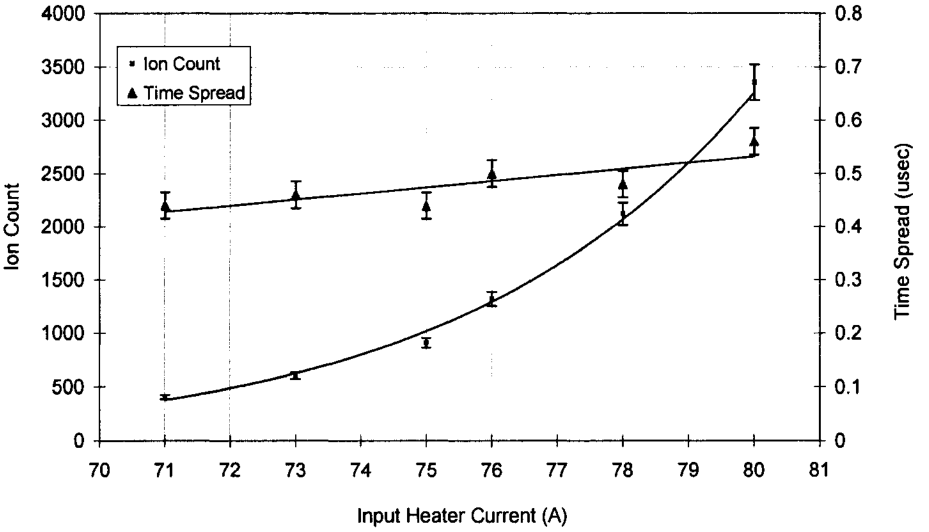

Figure 5.11 Effects of increased beams currents on the number of detected ions and their time spread. The data points were taken at 2400V_{RF} and -50V_{DC} axial well depth. The trendlines were generated using a polynomial fit to the data points.

5.6 Ion Temperatures

Using the HVTrap computer model outlined in chapter 4, ion signals were reproduced in order to determine the equilibrium temperatures achieved by confined ion ensembles at given operating conditions. In cases where ion pulses showed signs of bulging the main body of the signal was fitted while the tail-end of the pulse was ignored.

Figure 5.12 shows the variation of the ion temperature with the number of detected ions. This variation corresponds to the variation of pulse width shown in figure 5.11. The results shown in this figure are the most significant of the present work in that they show a minimum temperature of 0.45 ±0.05eV with an increase of 0.25±0.03 eV/1000 ions detected by the MCP detector. Taking the detection efficiency to be 0.5±0.2, the temperature increase with number of trapped ions is 0.12±0.03 eV/1000.

As a check on whether the ions had reached an equilibrium temperature before extraction, temperature calculations were also carried out for collections extracted after shorter collection times for ion loading rates that corresponded to 1500 detected ions after 500 ms of loading. The results are shown in figure 5.13.

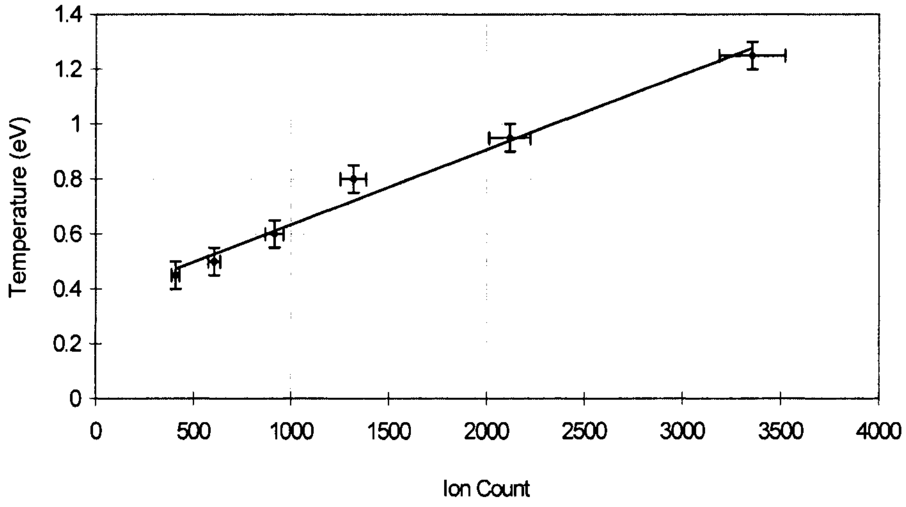

Figure 5.12 Simulated temperatures for larger ion ensembles at 2400V_{RF} and -50V_{DC} axial well depth. The trendline was generated using a linear fit to the data points.

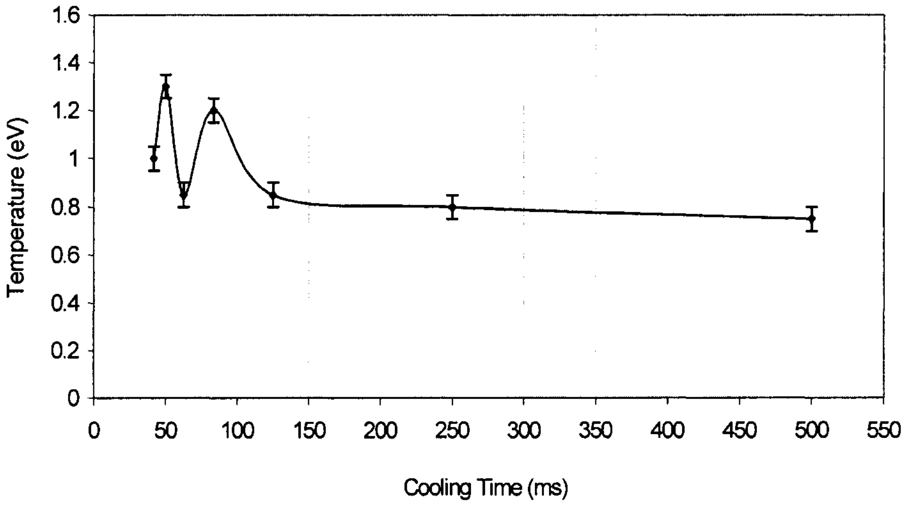

Figure 5.13 Simulated equilibrium temperatures of ion ensembles at shorter collection periods.

The results in figure 5.13 show erratic behaviour of the temperature if the ions are extracted before 100 ms of loading but that after 150 ms the temperature is stable.

Compared to the results of Kim and Fong, who used RFQ fields that were from 25 to 50 times weaker than those of the present work, the temperature shown in figure 5.12 are of the order of 10 times higher. At first, this might seem reasonable, considering the much higher quadrupole field strengths in the present work. In addition, the ions are only about 3 mm from electrodes that are oscillating to potential amplitudes of 2400 V at 7.5 MHz. Indeed, it is amazing that they pick up less than 1 eV of thermal energy.

While apparently small, 1eV of thermal energy is indeed commensurate with the size of the ion cloud, which from equations (2.40) is about 1.2 mm in diameter and 3 mm long (out to 2 sigma in density). While the quadrupole potential will be oscillating with an amplitude of about 50 V at the radial edge of this collection, the driven oscillation of the ions at this edge will have an average kinetic energy of only about 2 eV, and even this does not directly contribute to the thermal energy of the collection since it is coherent motion.

Yet it is still not clear how the ions pick up even this small thermal energy. If they are sitting in a pure quadrupole field they will oscillate about the point at which the field is zero and the buffer gas will remove the energy of these oscillations until the ions are sitting at this point. The only thing that will push the ions out into the RF field will be their mutual space charge repulsions. For the ion loadings of the trap at which the temperatures were measured, estimated to be of the order of twice the detected number, equations (2.52), (2.53) and (2.60) indicate that these effects could only make the ion cloud about 0.1 mm in diameter, which would lead to ion temperatures similar to those observed by Kim and Fong. For the space charge to account for the size of the ion collection, and therefore its temperature, there would have to be about 10 times as many ions in the collection as observed at the detector. In light of the tests carried out in the experiments, this seems very unlikely.

It seems then that the thermal energy of the ions must come from some component of a time-varying electric field that is driving the ions while they are sitting at the center of the quadrupole. This could not be a dipole component of the basic RF quadrupole field, which is easily obtained by an imbalance of the potential on the electrodes, since such a dipole can be eliminated by simply shifting the center of the ion collection to the point where the radial slope of the potential is indeed zero. (This was tested by deliberately unbalancing the electrodes by tuning the variable capacitors. There was no detectable effect on the ion temperature.)

However, dipole components of harmonics of the basic RFQ field could be present at the zero slope point of the quadrupole field. The presence of such components in the resonant circuit is shown by the frequency spectrum of the potentials that actually occur on the quadrupole electrodes. Such a spectrum, obtained by a frequency analyzer, is shown in figure 5.14.

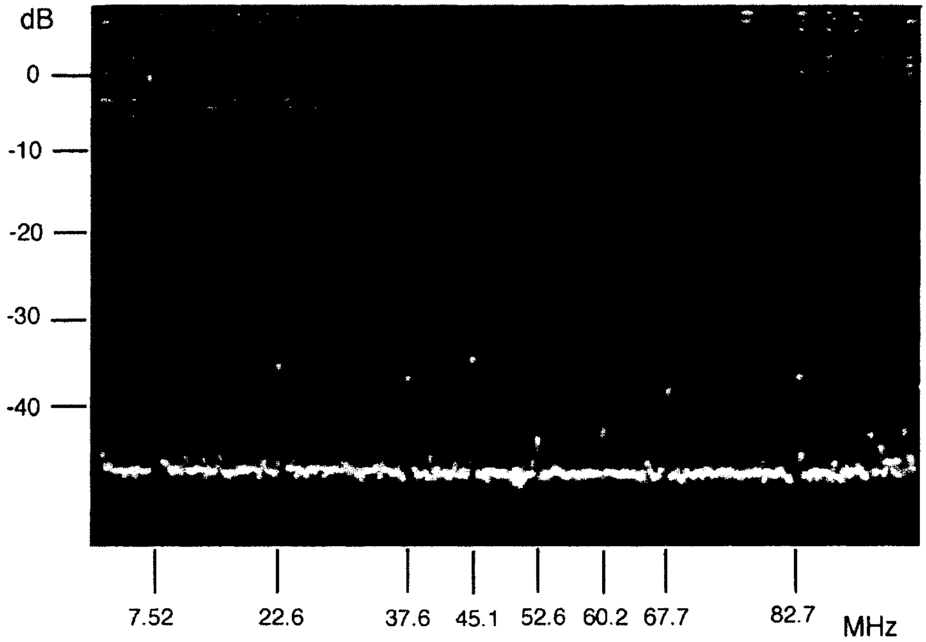

Figure 5.14 Frequency spectrum at $3850V_{RF}$. The first peak from the left is the main resonant frequency at 7.5MHz while the other smaller peaks are harmonics.

In this spectrum it is seen that the 3rd, 5th, 6th, 9th and 11th harmonics are all more about 2% of the fundamental RF signal at 7.52 MHz. Thus at 2400 V amplitude of the fundamental, the amplitudes of these high-frequency components were about 50 V each.

With the resonant circuit tuned to the fundamental, there is no reason to expect that these higher harmonics are in phase or in balance across the electrodes. Thus they could present fields at the center of the quadrupole that will cause heating of the ion collection.

Efforts to reduce the harmonics by capacitive filtering at the autotransformer feeding the resonant coils failed. However, measurements were made of the harmonic content of the amplifier output at various power levels. The results are shown in table 5.2.

Harmonic	1200 V_{RF}	1930 V_{RF}	2650 V_{RF}	3370 V_{RF}	4100 V_{RF}
2	--	-47 dB	--	--	--
3	-40 dB	-39 dB	-38 dB	-36 dB	-35 dB
4	--	--	--	--	--
5	-43 dB	-42 dB	-40 dB	-37 dB	-36 dB
6	-39dB	-38 dB	-37 dB	-35 dB	-34 dB
7	--	--	-47 dB	-45 dB	-44 dB
8	--	-49 dB	-48 dB	-45 dB	-46 dB
9	-42 dB	-43 dB	-41dB	-38 dB	-38 dB
10	-30 dB	--	--	--	--
11	--	-41 dB	-38 dB	-36 dB	-38 dB

Table 5.2 List of the resonant harmonics and their relative strength at different RF voltages. The decibel values are relative to the main resonant frequency at 7.5 MHz (ex. At 4100V_{RF}, the 11th harmonic is 37.5 dB lower than the main signal found at 7.5MHz). All measurements were taken with a ±2dB error.

This shows that the harmonic content is generally increased at higher output levels. Consequently, some temperature measurements were therefore carried out at higher RF levels. The results are shown in figure 5.15.

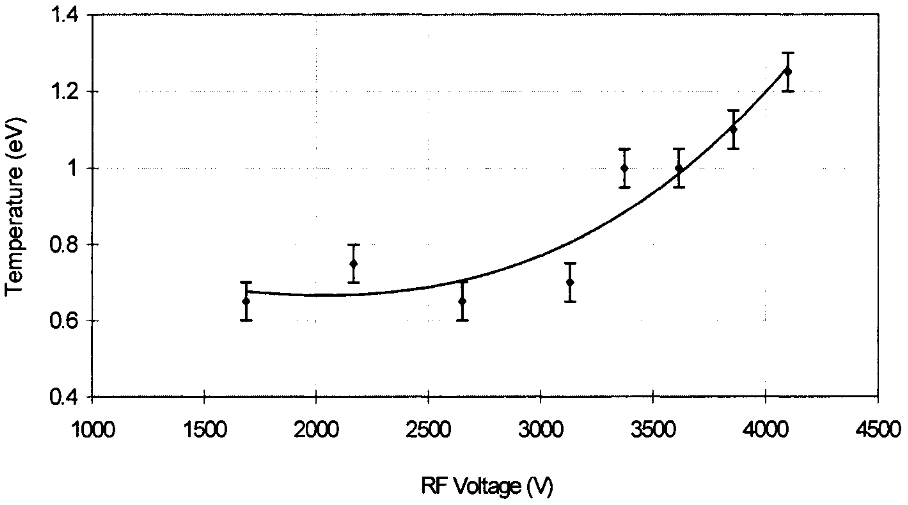

Figure 5.15 Simulated equilibrium temperatures of ion ensembles at various RF settings. The trendline was generated using a polynomial fit to the data points.

The increased temperature at the higher RF fields does not prove, however, that the RF harmonics are solely responsible. It is suggested that further work should be carried out using a resonant circuit that is not subject to harmonic distortion so as to eliminate the possibility of such harmonics heating the ion collection.

Also as further work, a detector should be implemented at the exit of the trap extraction electrode so that all the ions exiting the trap can be counted. This would eliminate the possibility that there is an error in estimating the number of ions in the trap.

5.7 Implications for TOF Mass Spectrometry

With even the best modern electronics and computer analysis of data, the largest single collection of ions that can be analyzed for mass in a modern TOF mass spectrometer numbers about 1000, at a repetition rate of 10 Hz. Figure 5.13 shows that this repetition rate is feasible with a linear trap and the results presented in figure 5.12 show that a high-field RFQ linear trap can contain a collection of about 1000 cesium ions in an axial extent of about 3 mm at a temperature of about 0.5 eV. The action diagram of this collection, including only the ions that will contribute to the TOF signal within a range of full-width half maximum, i.e., $\pm 1.2\sigma$, will be about 2 eV-μs. From equation (2.62), a TOF mass spectrometer that can accommodate a typical energy spread of 100 eV and provide a flight time of 40 μs for 133 amu ions, (also typical) , would have a mass resolution of about 1000. Since both the action area and the time of flight of the ion are both proportional to the square root of the ion mass, (2.62) shows that this mass resolution would be independent of the ion mass.

For such a spectrometer the energy spread of 100 eV would be achieved by applying an extraction field of 33 V/mm over the 3 mm length of the ion collection. However, in designing a linear trap as a source for a TOF mass spectrometer, rather than as in the present work as a tool for probing the phase space density of the trapped ions, the axial confinement would be strengthened so that the collection would be about 1 mm in axial extent. This would be achieved by increasing the angular velocity of the axial oscillation by a factor of 3, resulting in decrease the axial action area by a factor of 3. The extraction field at the collection would then have to be about 100 V/mm but the mass resolution that results would be about 3000. This would make it competitive with most other TOF mass spectrometers. The great advantage of the linear trap as a source for TOF mass spectrometry is that it can use a continuous source, thereby greatly expanding the range of sources that can be used.

Dreaming a little, if it becomes possible, by refining and stabilizing the RF supply, to reduce the ion temperature to the 0.05 eV achieved by Kim and Fong, then a TOF spectrometer using such a linear trap as a source could achieve a mass resolution (FWHM) of 30,000. This would make it competitive with the present top of the line TOF mass spectrometers for biomolecular research based on Matrix Assisted Laser Desorption Ionization (MALDI), a process that requires extensive preparation of the samples to be ionized and which is inherently unstable.

5.8 Implications for High-Field RFQ Beam Cooling

The principle implications of the present results for ion beam cooling using high-field RFQ confinement in a buffer gas is that it is possible and that ion temperatures at least as low as 1 eV are possible. However, the results do not seem to give a means of estimating the ion currents that can be accommodated. This is because the ion densities that were feasible in the present work were only about 2000 cesium ions per millimeter of axial extent of the collection. Such a density over a long axial confinement in which the ions were dragged at 1 mm/μs, would result in a beam current of only about 300 pA. Kim, using a RFQ field of about 25 times less than that of the present work, could transport ions currents of up to 1.2 nA at temperatures of only 70 meV. From the space-charge consideration of chapter 2 leading to equation (2.50), one would expect that the beam current that could be contained would scale as the square of the macromotion frequency resulting from the confinement. The macromotion frequency in the confinement used in the present work was about 10 times that used by Kim, so it would be expected that up to 100 nA of beam could be confined. Clearly, to determine the continuous beam that can be confined, a linear RFQ system must be built that can accommodate such a beam.

Chapter 6 Conclusion

This thesis has proven that high-field RFQ confinement of ions in a buffer gas is feasible and that manipulation of such ions by DC fields is feasible by applying the necessary potentials through shields that provide the RF to the electtodes. Operation at up to 4100V RF amplitude between electrodes that are separated by only 1 mm at their closest approach has been demonstrated. These potentials were maintained at helium buffer gas pressures of up to 10^{-4} Torr. With a separation between facing electrodes of 6.25 mm for the axiperiodic quadrupole of the containment device and an applied RF of 7.5 MHz, the angular frequency of the simple harmonic motion of cesium ions due to the radial confinement at 2400 V amplitude RF was 7.0 rad/μs (1.1 MHz).

Under these operating conditions, ion collections were extracted from the trap for time-of-flight analysis. This showed that up to about 10,000 ions could be collected in a diameter of about 1 mm and an overall length of 3 mm. The temperatures of the ion collection were about 1 eV or less, depending on the number of ions in the trap. The source of the heating is, possibly, impurity of the RF applied to the confining electrodes.

The main contributions of the thesis are the principles by which RFQ confinement can be engineered for specific purposes, such as for an ion source of a high-resolution TOF mass spectrometer or for the cooling of intense ion beams by buffer gas. It is suggested that further work should be carried out to build prototypes of such apparatus.

6.1 Suggested Development of a TOF Mass Spectrometer

An RFQ linear trap for practical TOF mass spectrometry would have a geometry similar to that of the present work but with a shorter middle trapping section and with the possibility of higher extraction potentials on the end electrodes, possibly up to ±3 kV. With such a design it should be possible to contain the ions in a tighter axial geometry and still extract them with the appropriate energy spread to maximize the TOF mass resolution. Design should be carried out with adequate numerical simulation of the TOF signal so that the mass resolution can be optimized. Of course, an appropriate reflectron should be incorporated in the design.

Also, for practical TOF mass spectrometry using a particular ion source, an appropriate ion delivery system must be incorporated. For continuous ion beams this would be an RFQ ion guide, matched to the RFQ linear trap. This would be most easily accomplished by using the same RF supply for both the guide and the trap, where the trap, as in the work of Fong, is just a continuation of the RFQ guide but with the appropriate change in axial length of the electrode segments and the applied DC potentials. A schematic of the suggested apparatus is shown in figure 6.1

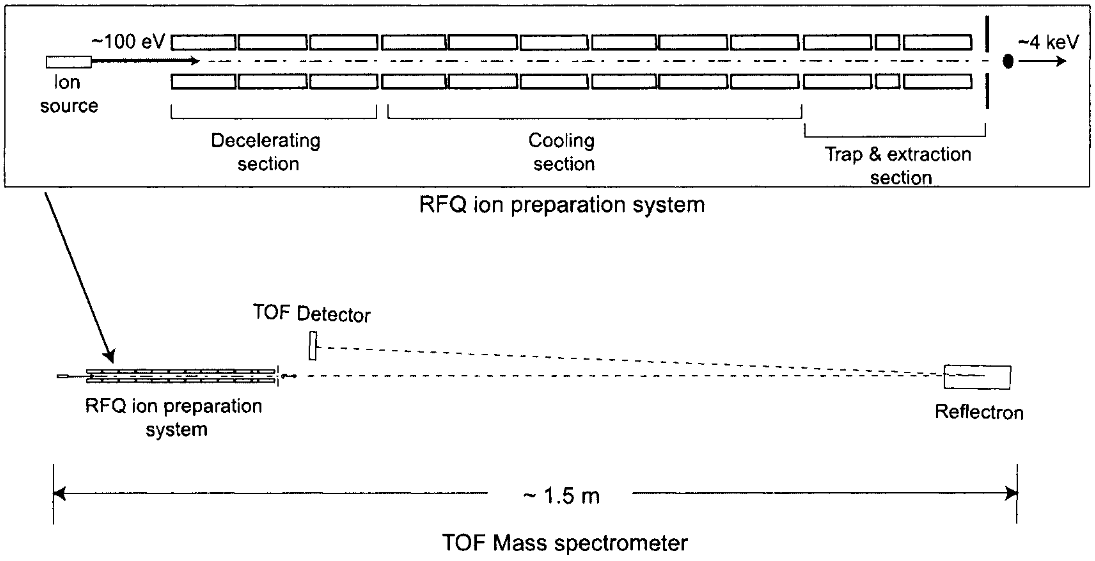

Figure 6.1 Schematic of a suggested TOF mass spectrometer. It is believed the RFQ ion preparation system could be designed to have an overall length of no more than 300 mm, with the overall length of the spectrometer being of the order of a 1.5 meters.

As suggested already in chapter 5, this development should include a high stability purely sinusoidal RF supply and a better resonating circuit to generate high RF potentials.

6.2 Suggested Development of a High-Field Beam Cooling Device

A high-field cooling device for high current ion beams would require significant developmental work on the deceleration of the beams so that they could be made to enter the RFQ confinement region and on the subsequent extraction of the cooled beams so that they were not reheated upon exit from the system. Also, the RFQ confinement region should be designed for even higher RF potentials then in the present work and should be considerably extended over even that for a TOF mass spectrometer so that the ions encounter enough buffer gas to be adequately cooled.

It is felt that this would require the RFQ ion guide leading to a possible trap to be made up of three sections; one for capturing the ion beam delivered by an electrostatic decelerator and further decelerating it to a velocity that can be reduced to zero by the buffer gas, a second section that has buffer gas at sufficient pressure to stop the ions and cool them, after which it drags then the a third section where the buffer gas pressure is reduced so as to enable efficient extraction of the ions without subsequent heating by high-energy collisions with buffer gas molecules. Such a configuration is outlined in figure 6.2.

The design of such a system would require detailed computer simulation of the ion trajectories under a variety of operating conditions so as to optimize the performance and to minimize the pumping requirements. Also, as for the RFQ ion preparation system, an RF system should developed that has better stability and purity than the system used in the present work. For a beam cooler it is suggested that two back-to-back ¼ wave resonators be employed to provide the necessary RF potentials. This would provide a closed resonant circuit that would not be subject to radiation losses that significantly reduce the quality factor Q of the resonating circuit. This technique has already been employed in work with a miniature RFQ trap at NIST in Colarado [Jef95], where a Q of up to 4000 has been achieved.

This technique in itself would require higher RF potentials since the operating radiofrequency would probably have to be increased in order to make such a resonating system feasible.

Finally, experience with electrode mounting system of the present work shows that there would be great benefit in having a rigid mounting system for the back-bones delivering the RF, rather than having them mounted in a fashion that required accurate alignment to achieve electrode symmetry. A suggested mounting system is outlined in figure 6.3.

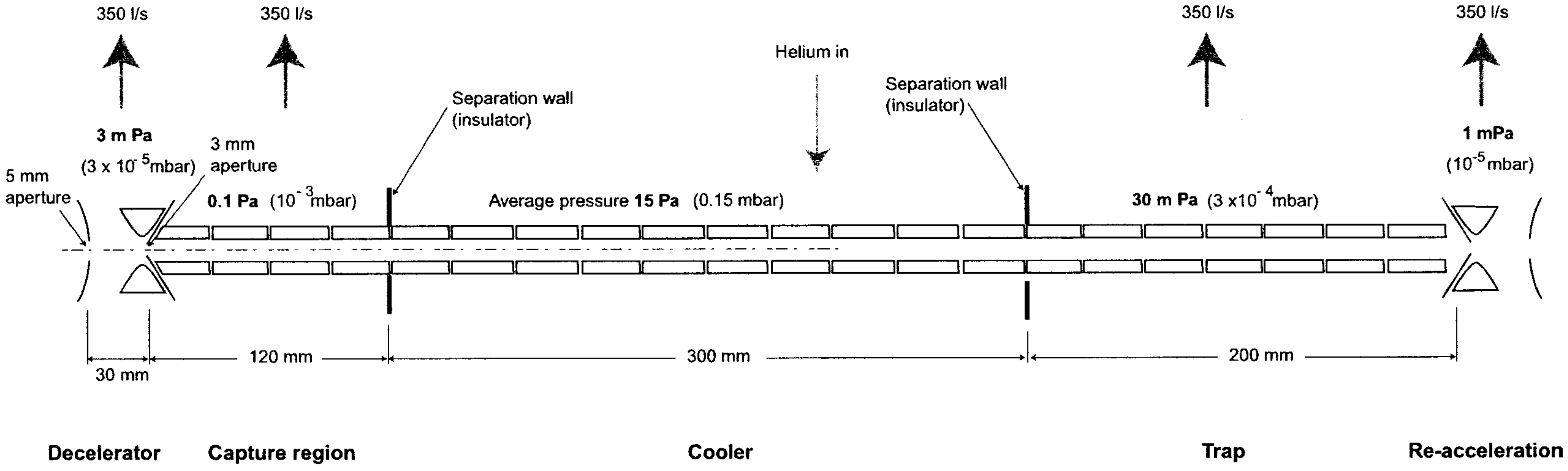

Figure 6.2. The basic components of a high-performance beam cooler-buncher based on RFQ confinement in a buffer gas. The segment lengths shown in the drawing are not representative of the actual lengths that will be used, particularly in the cooler and trapping regions, where they will have to be no longer than 10 mm each.

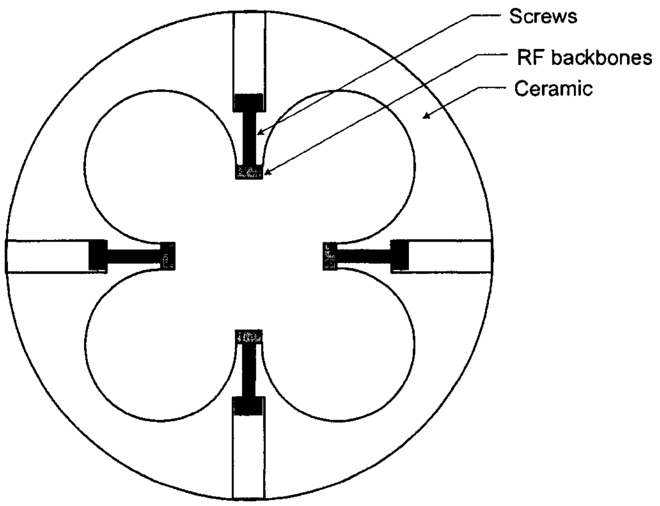

Figure 6.3 Suggested insulating mounts for the RF backbones of a high-field ion beam cooler.

It is highly recommended, based on the experience of other workers with high electric fields on insulting surfaces in a vacuum, that all insulators in any such system be ground from high purity alumina, rather than machined from “machinable” ceramics. This is because the jagged surfaces of such ceramics, easily seen under a jeweler’s eyeglass, do not provide a stable insulation against high RF fields and can lead to cracks that provide easy paths for electrical discharges. Also, of course, all electrode surfaces, particularly those that are exposed to high electric fields should be highly polished. Although not employed in the electrodes of the present work, where the electrodes were hand polished with optical rouge, electro-polishing is recommended.

The work of this thesis has led to the fervent hope that the development of such high-powered RFQ confinement devices will significantly enhance the art of ion manipulation for accurate and sensitive experiments in physics, chemistry and biology.

References

[Als68] Alston, L.L. High Voltage Technology. London: Oxford University Press, 1968.

[Ber98] Berkeland, D.J., et al., Methods for Ultrasensitive Detection, edited by B.L. Fearey, SPIE, Bellingham, WA, 1998.

[Beu74] Beukema, G.P. “Effects of Clumps and Ion Bombardment on Electrical Breakdown in Vacuum.” J. Phys. D: Appl. Phys. 7, 1740 (1974).

[Bol96] Bollen, G., Becker, S. Kluge, H.-J., Konig, M., Moore, R.B., Otto, T., Raimbault-Hartman, H., Savard, G., Schweikhard, L., Stolzenberg, H., “Isoltrap: a tandem Penning trap system for accurate on-line mass determination of short-lived isotopes.” Nuclear Instruments and Methods in Physics Research A, 368, 675 (1996).

[Bug96] Bugg, D.V. Electronics: Circuits, Amplifiers and Gates. Philadelphia: Institute of Physics Publishing, 1996.

[Cha67] Charbonnier, F.M., C.J. Bennette, L.W. Sawnson. “Electrical Breakdown Between Metal Electrodes in High Vacuum.” J. Appl. Phys. **38**, 627 (1967).

[Che99] Chernushevich, I.V., Ens, W., Standing, K.G., “Orthogonal Injection TOFMS for Analyzing Biomolecules.” Analytical Chemistry News & Features July1, 1999 (1999): 452-461.

[Chi97] Chikazumi, S. Physics of Ferromagnetism. New York: Clarendon Press Oxford, 1997.

[Daw76] Dawson, P.H. Quadrupole Mass Spectrometry and Its Applications. Amsterdam: Elsevier Scientific Publishing Company, 1976.

[Deh67] H.G. Dehmelt, Advan. At. Mol. Phys., 3 (1967) 53.

[Dou05] Douglas, D.J., Frank, A.J., Dunmin, M., "Linear Ion Traps in Mass Spectrometry." Mass Spectrometry Reviews 24, 1-29 (2005).

[Eij99] Eijkelenborg, M.A., Storkey, M.E.M., Segal, D.M., Thompson, R.C., "Ion Dynamics in a Novel Linear Combined Trap", International Journal of Mass Spectroscopy 188, 155-161 (1999)

[Fon01] Fong, C.W.V. "Phase Space Dynamics in a Linear RFQ Trap for Time – of-Flight Mass Spectrometry." Ph.D. Thesis, McGill University. 2001.

[Gha96] Ghalambor-Dezfuli, A.M. "Injection, Cooling, and Extraction of Ions from a Very Large Paul Trap." Ph.D. Thesis, McGill University.1996.

[Gia02] Gianfrancesco, O., "Design Principles of a High Field RFQ Device for Ion Cooling and Confinement." Master's Thesis, McGill University. 2002.

[Gua94] Guan, S., Marshall, A.G., "Equilibrium Space Charge Distribution in a Quadrupole Ion Trap". J. Am. Soc. Mass Spectrom., 5, 64-71 (1994).

[Hao01] Hao, C., March, R.E., "A Survey of Recent Activity in Quadrupole Ion Trap Mass Spectrometry", International Journal of Mass Spectrometry 212, 337-357 (2001).

[Hal88] Halliday, D., R. Resnick, and J. Merrill, textbook. *Fundamentals of Physics.* USA: John Wiley & Sons, 1988.

[Her01] Herfurth, F., Dilling, J., Kellerbauer, A., Bollen, G., Henry, S., Kluge, H.-J., Lamour, E., Lunney, D., Moore, R.B., Scheidenberger, C., Schwarz, S., Sikler, G., Szerypo, J., "A Linear Radiofrequency Ion Trap for Accumulation, Bunching and Emittance Improvement of Radioactive Ion Beams", Nuclear Instruments and Methods in Physics Research A 469, 254-275 (2001).

[Hop99] Hopfgartner, G., Chernushevich, I., Covey, T., Plomley, J.B., Bonner, R., "Exact Mass Measurement of Product Ions for theStructural Elucidation of

Drug Metabolites with a Tandem Quadrupole Orthogonal-Acceleration Rime-of-Flight Mass Spectrometer." J. Am. Soc. Mass Spectrom. 10 (1999): 1305-1314.

[Hor97] Horvath, G. Zs. K., Thompson, R.C., Knight, P.L., "Fundamental Physics with Trapped Ions", Contemporary Physics 38, 25-48 (1997).

[Hou00] Hou, J., Wang, Y., Yang, D., "The Properties of Ion Clouds in a Paul Trap: A Statistical Model", Journal of Applied Physics 88, 4334-4339 (2000).

[Hub61] Hubert, C.I. Operational Electricity: Theory, Characteristics, Application, and Mode of Operation of Circuits and Machines. New York: John Wiley & Sons, 1961.

[Jef95] Jefferts, S.R., Monroe, C., Bell, E.W., Wineland, D.J., "Coaxial-Resonator-Driven RF (Paul) Trap for Strong Confinement", Physical Review A 51, 3112-3116 (1995).

[Kel01] Kellerbauer, A., Kim, T., Moore, R.B., Varfalvy, P., "Buffer Gas Cooling of Ion Beams", Nuclear Instruments and Methods in Physics Research A 469, 276-285 (2001).

[Kil57] Kilpatrick, W.D. "Criterion for Vacuum Sparking Designed to Include Both RF and DC." Review of Scientific Instruments **28**, 824 (1957).

[Kim97] Kim, T. "Buffer Gas Cooling of Ions in a Radio Frequency Quadrupole Ion Guide." Ph.D. Thesis, McGill University. 1997.

[Kin24] Kingdon, K.N., and J. Langmuir, 1924.

[Lat81] Latham, R.V. High Voltage Vacuum Insulation: The Physical Basis. London: Academic Press, 1981.

[Law83] Lawson, J.D. "Space Charge Optics." Chap. in *Applied Charged Particle Optics*. 2. USA: Academic Press, Inc., 1983.

[Lob03] Loboda, A.V., Ackloo, S., Chernushevich, I.V., "A High-Performance Matrix-Assisted Laser Desorption/Ionization Orthogonal Time-of-Flight Mass Spectrometer with Collisional Cooling." Rapid Commun. Mass Spectrom. 2003; 17: 2508–2516

[Loe39] Loeb, L.B. Fundamental Processes of Electrical Discharge in Gases. New York: John Wiley & Sons, 1939.

[Lun92] Lunney, M.D.N. "The Phase Space Volume of Ion Clouds in Paul Traps." Ph.D. Thesis, McGill University. 1992.

[Maj68] F.G. Major and H.G. Dehmelt, Phys. Rev., 170 (1968) 91.

[Mar95] March, R.E., Todd J.F.J. "Modern Mass Spectrometry - Practical Aspects of Ion Trap Mass Spectometry." CRC Press series, 1995.

[Mar97] March, R. E., "An Introduction to Quadrupole Ion Trap Mass Spectrometry", Journal of Mass Spectrometry 32, 351-369 (1997).

[Mou55] Moullin, E.B. The Principles of Electromagnetism. London: Oxford at The Clarendon Press, 1955.

[Oka02] Okamoto, H., Ito, K., Takai, R., Wada, Y., "A New Experimental Approach to Space Charge Effects", Porceedings of EPAC 2002.

[Pau53] W. Paul and H Steinwedel, Z. Naturforsch, A, 8 (1953) 448.

[Pla03] Plass, W. R., Hongyan, L., Cooks, R.G., "Theory, Simulation, and Measurement of Chemical Mass Shifts in RF Quaddrupole Ion Traps", International Journal of Mass Spectrometry 228, 237-267 (2003).

[Sin80]	Sinha, M.K., Y. Ku, R.P. Randall. "Surface Damage on Stainless Steel and Molybdenum Electrodes Caused by Electrical Breakdown in High Vacuum." J. Appl. Phys. **52**, 699 (1980).
[Spo27]	Spooner, T. Properties and Testing of Magnetic Materials. New York: McGraw-Hill Book Company, 1927.
[Tan96]	Tanner, D., Jefferson, A., Eisele, F.,"Selected Ion Chemical Ionization Mass Spectrometry Measurements of OH", J. Geophysics. Res., 14, 665 (1996).
[Tod99]	Todd, J. F. J., "A Retrospective Review of the Development and Application of the Quadrupole Ion Trap Prior to the Appearance of Commercial Instruments", International Journal of Mass Spectrometry 190/191, 9-35, (1999)
[Vie75]	L.A. Viehland, E.A. Mason, W.F. Morrison and M.R. Flannery, Atomic and Nuclear Data Tables **16** (1975) 495.
[Won97]	Wong, P.S.H., Cooks, R.G., Ion Trap Mass Spectrometry, Bioanalytical Systems Inc., 16, (1997).
[Wue59]	R.F. Wuerker, H. Shelton and R.V. Langmuir, J. Appl. Phys., 30 (1959) 342.
[Yar67]	Yarwood, Y. High Vacuum Technique. London: Chapman and Hall, 1967.

Appendix A

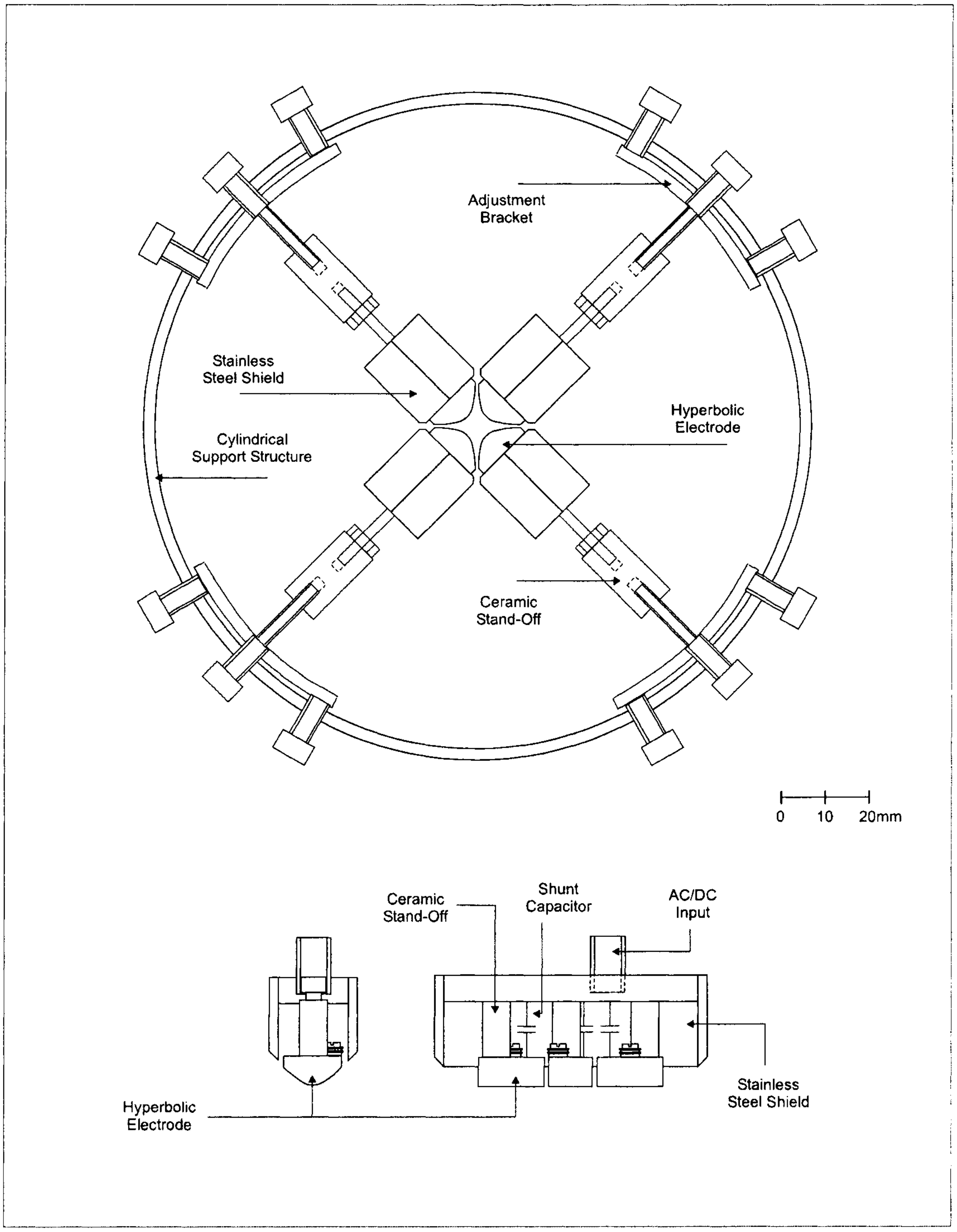

Figure A.1 **HVTrap assembly.**

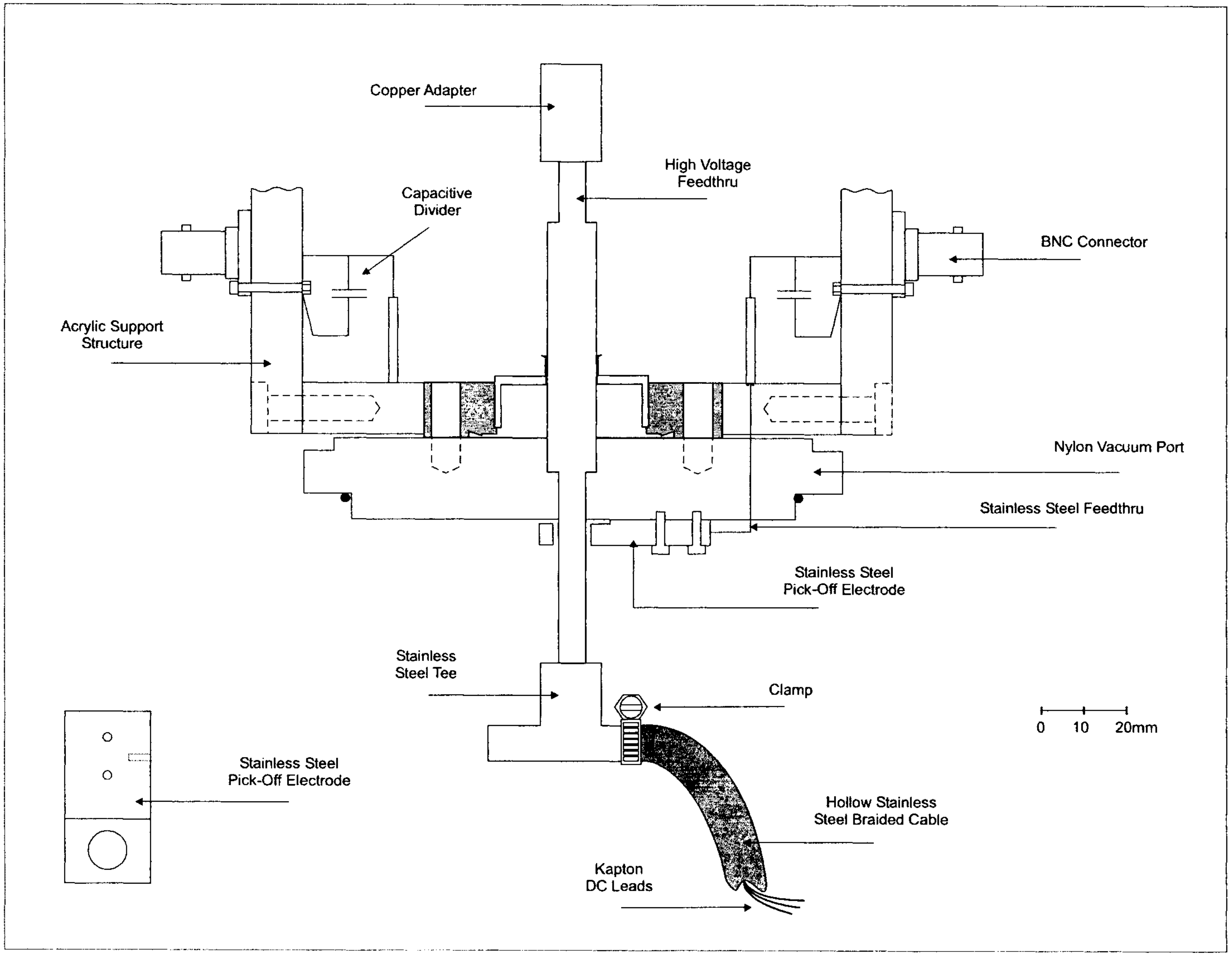

Figure A.2 High voltage feedthrough assembly.

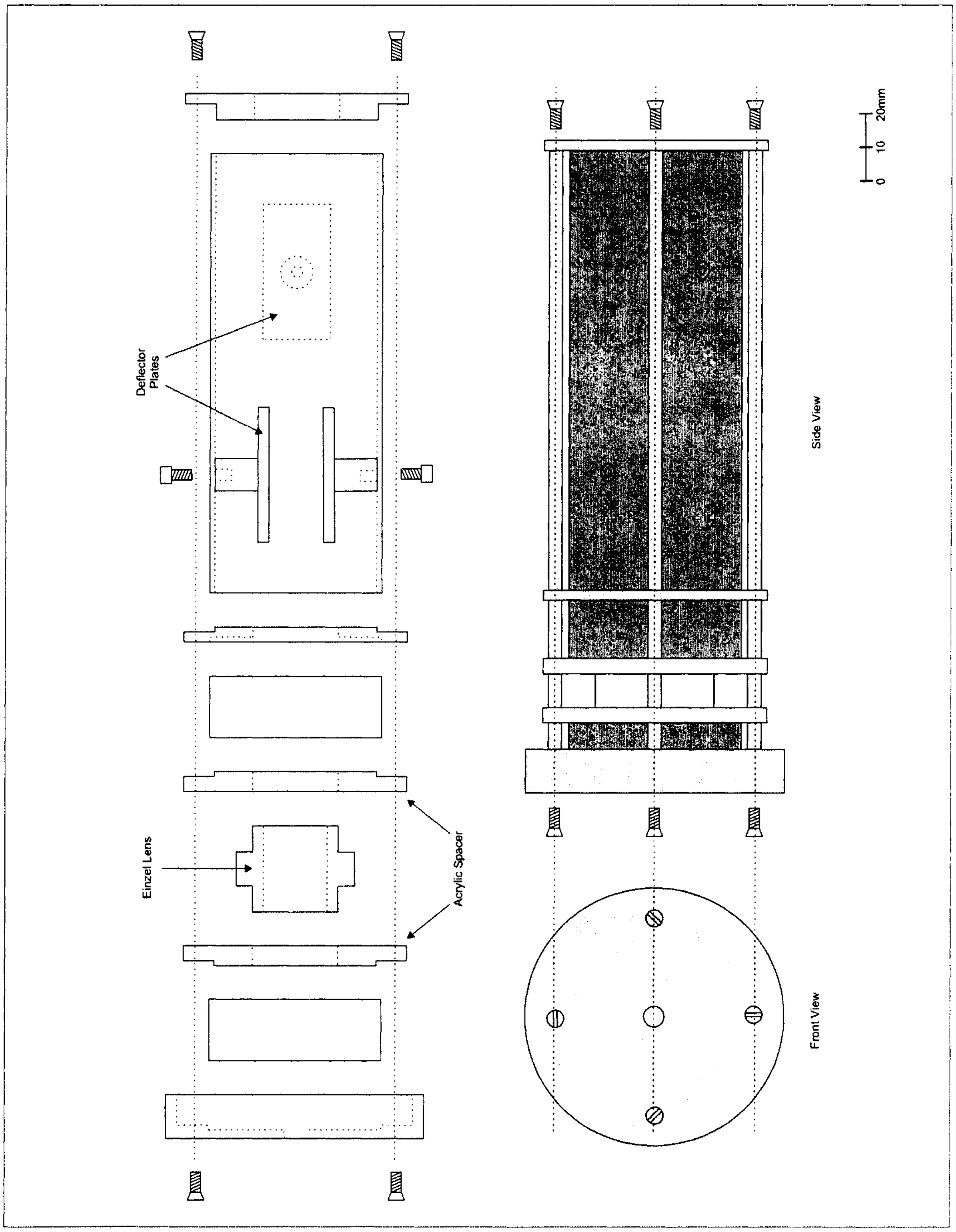

Figure A.3 Einzel lens and deflector plate assembly